

**Zn and Cu Co-Doped $\text{Li}_4\text{Ti}_5\text{O}_{12}$ Anode Material for Lithium Ion
Batteries**

by

Md. Mehedi Hasan

ID:1653555

A thesis submitted in fulfillment of the requirements for the degree
of Master of Science in Chemistry



Khulna University of Engineering & Technology

Department of Chemistry

June 15, 2019

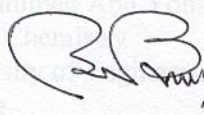
**Dedicated
To
My Beloved Parents**

Declaration

This is to certify that the thesis work entitled “Zn and Cu Co-Doped $\text{Li}_4\text{Ti}_5\text{O}_{12}$ Anode Material for Lithium Ion Batteries” has been carried out by Md. Mehedi Hasan in the Department of Chemistry, Khulna University of Engineering & Technology, Khulna, Bangladesh. The above thesis work has not been submitted anywhere for the award of any degree or diploma.

BOARD OF EXAMINERS

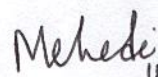
Signature of Supervisor



15/06/19

Prof. Dr. Mohammad Abu Yousuf
Department of Chemistry
Khulna University of Engineering &
Technology
Khulna-9203, Bangladesh

Signature of Candidate



15/06/19

Md. Mehedi Hasan
Roll No.:1653555
Department of Chemistry
Khulna University of Engineering &
Technology
Khulna-9203, Bangladesh

Prof. Dr. Md. Mizanur Rahman Babel
Department of Chemistry
Khulna University of Engineering & Technology


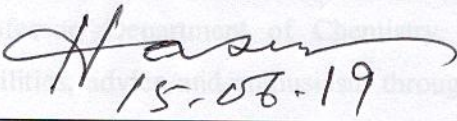
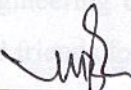
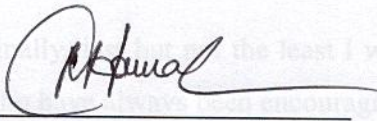
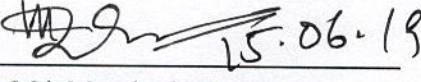
Dr. A. B. M. Mamun Jamal
Assistant Professor
Department of Chemistry
Khulna University of Engineering & Technology

Dr. Md. Moinul Islam
Associate Professor
Department of Chemistry
University of Dhaka

Approval

This is to certify that the thesis work submitted by Md. Mehedi Hasan entitled “**Zn and Cu Co-doped $\text{Li}_4\text{Ti}_5\text{O}_{12}$ Anode Material for Lithium Ion Batteries**” has been approved by the board of examiners for the partial fulfillment of the requirements for the degree of M.Sc. in the Department of Chemistry, Khulna University of Engineering & Technology, Khulna, Bangladesh.

BOARD OF EXAMINERS

1.  15/06/19
Prof. Dr. Mohammad Abu Yousuf
Department of Chemistry
Khulna University of Engineering & Technology
Chairman
(Supervisor)
2.  15.06.19
Head
Department of Chemistry
Khulna University of Engineering & Technology
Member
3. 
Prof. Dr. Md. Mizanur Rahman Badal
Department of Chemistry
Khulna University of Engineering & Technology
Member
4. 
Dr. A. B. M. Mamun Jamal
Assistant Professor
Department of Chemistry
Khulna University of Engineering & Technology
Member
5.  15.06.19
Dr. Md. Mominul Islam
Associate Professor
Department of Chemistry
University of Dhaka
Member
(External)

Acknowledgements

All the admirations are for almighty Allah, who helped me in difficulties and gave me enough strength and ability to accomplish this research work.

First and foremost I would like to extend my sincere gratitude to my thesis advisor **Dr. Mohammad Abu Yousuf**, Professor, Department of Chemistry, Khulna University of Engineering & Technology. I thank him immensely for his excellent guidance, support and valuable suggestions throughout this endeavor, which nurtured a lot of confidence in me.

I would like to thank Prof. Dr. Mohammad Hasan Morshed, Head, the Department of Chemistry, KUET and the staff of the department for their continuous support during my thesis work. I would like to give my special thanks to Parbhej Ahmed, Assistant Professor, Department of Chemistry, KUET for his excellent support, laboratory facilities, advice and enthusiasm throughout my M.Sc. I am indeed grateful to all my dear teachers of the Department of Chemistry, KUET who triggered my interest in the subject and was my real inspiration for doing research.

I would like to thank University Grant Commission and Khulna University of Engineering & Technology for funding my research. I sincerely thank all my labmates and friends for their sincere co-operation and encouragement.

Many thanks to Samina Ahmed, Director (In-charge), Dhaka Laboratories, BCSIR, Dhanmondi, Dhaka for the assistance concerning the XRD and SEM-EDX measurement of LTO composites.

Finally, last but not the least I would like to thank my parents and my family members who have always been encouraging me in all aspects of life.

Md. Mehedi Hasan

ABSTRACT

Lithium-ion batteries have advanced the battery technology because of their prevalent power sources for electric vehicles and portable electronics devices. Spinel structure of lithium titanium oxide $\text{Li}_4\text{Ti}_5\text{O}_{12}$ (LTO) has commended significant interest as an anode material for lithium-ion batteries because of several advantages such as high energy density, high safety, good chemical stability, long-life time, a flat operating voltage about 1.55 V and low cost. Modification of the surface structure of LTO based anode material by Cu and Zn has been significantly enhanced the conductivity of the electrode material by suppressing the decomposition of the electrode material and influencing their phase structure in some cases. Advanced spectroscopic techniques, such as Fourier-Transform Infrared Spectroscopy (FTIR), scanning electron microscopy (SEM), (EDX) and X-ray diffraction (XRD) are applied for the characterization of morphology, particle size and crystal structure of the prepared LTO based anode materials.

In the finger print region sharp low frequency characteristic IR bands observed below 800 cm^{-1} which can be attributed to the symmetric stretching vibrations of Ti-O bonds of TiO_6 octahedron in pure $\text{Li}_4\text{Ti}_5\text{O}_{12}$, $\text{Li}_4\text{Ti}_{4.9}\text{Cu}_{0.05}\text{Zn}_{0.05}\text{O}_{12}$, $\text{Li}_{3.9}\text{Ti}_5\text{Cu}_{0.05}\text{Zn}_{0.05}\text{O}_{12}$ and $\text{Li}_{3.9}\text{Ti}_{4.9}\text{Cu}_{0.1}\text{Zn}_{0.1}\text{O}_{12}$. At the same time strong stretching bands at around 2360.87, 2341.58 and 2331.94 cm^{-1} can be assigned to the Ti-O-Ti bonds in the prepared LTO and LTO based anode materials and corresponds to the published results.

$\text{Li}_4\text{Ti}_5\text{O}_{12}$ possess a face-centered cubic spinel structure grounded on space group symmetry of Fd3m. In the $\text{Li}_4\text{Ti}_5\text{O}_{12}$ spinel structure, tetrahedral 8a sites are completely taken up by Li and the octahedral 16d sites are arbitrarily occupied by Li and Ti with an atomic ratio of 1:5 in a cubic close-packed oxygen array. The characteristic X-ray diffraction peaks of the prepared samples are found at 2θ of 18.3, 35.58, 43.2449, 43.1, 57.2065, 62.8447, and 66.1006 which correspond to the planes (111), (311), (400), (333), (440) and (531), respectively. The lattice parameter values were calculated for $\text{Li}_4\text{Ti}_5\text{O}_{12}$, $\text{Li}_4\text{Ti}_{4.9}\text{Cu}_{0.05}\text{Zn}_{0.05}\text{O}_{12}$, $\text{Li}_{3.9}\text{Ti}_5\text{Cu}_{0.05}\text{Zn}_{0.05}\text{O}_{12}$ and $\text{Li}_{3.9}\text{Ti}_{4.9}\text{Cu}_{0.1}\text{Zn}_{0.1}\text{O}_{12}$ and the values are 8.3692 Å, 8.3742 Å, 8.3834 Å and 8.3709 Å, respectively. XRD spectra that both pure $\text{Li}_4\text{Ti}_5\text{O}_{12}$ and Cu & Zn co-doped LTOs showed peaks representing single phase of spinel lithium titanium oxide (cubic phase, space group Fd-3m) which are in good

agreement with Joint Committee on Powder Diffraction Standards, JCPDS (No. 26-1198) data.

SEM photographs of prepared pure LTO ($\text{Li}_4\text{Ti}_5\text{O}_{12}$), $\text{Li}_4\text{Ti}_{4.9}\text{Cu}_{0.05}\text{Zn}_{0.05}\text{O}_{12}$, $\text{Li}_{3.9}\text{Ti}_5\text{Cu}_{0.05}\text{Zn}_{0.05}\text{O}_{12}$ and $\text{Li}_{3.9}\text{Ti}_{4.9}\text{Cu}_{0.1}\text{Zn}_{0.1}\text{O}_{12}$ possess chips like shape. No significant change happened in the morphologies due to the co-doping of different ratio of Cu & Zn into $\text{Li}_4\text{Ti}_5\text{O}_{12}$. The morphologies of all prepared LTOs are almost same that correspond the X-ray diffraction result.

Contents

Title Page	Page I
Declaration	II
Acknowledgement	V
Abstract	VI
Contents	VIII
List of Tables	X
List of Figures	XI
List of Symbols and Abbreviations	XIII

CHAPTER I	Introduction	Page
	1.1 General	1
	1.2 Lithium Ion Batteries	1
	1.3 Lithium Ion Battery Components	2
	1.4 Opportunities in Lithium Ion Batteries	5
	1.5 Motivation for LTO as Anode Material	6
	1.6 Structure of LTO	7
	1.7 Phase Transition Behavior of $\text{Li}_4\text{Ti}_5\text{O}_{12}$ and $\text{Li}_7\text{Ti}_5\text{O}_{12}$	8
	1.8 Why Rechargeable Li-Ion Battery?	10
	1.9 Working Principle of Li-Ion Battery	11
	1.10 Cathode	13
	1.10.1 Layered Structured Cathode	14
	1.10.2 Spinel Structured Cathode	15
	1.10.3 Olivine Structured Cathode	15
	1.11 Anode	15
	1.11.1 Metallic Li Anode	16
	1.11.2 Carbonaceous Anode	16
	1.11.3 Sn and SnO_2 Based Anode	17

1.11.4 Lithium Titanate Anode	17
1.11.5 Other Metal Oxide Anode	18
1.11.6 Graphene-Based Anode	18
1.12 Various Methods of Synthesizing LTO	18
1.13 Synthesis of LTO Using Sol-gel Method	20
1.14 Characterization Ttechniques	22
1.14.1 Fourier-Transform Infrared Spectroscopy (FTIR)	22
1.14.2 X-ray Diffraction (XRD)	23
1.14.3 Scanning Electron Microscopy (SEM)	25
1.15 Electrochemical Characterization Using Cyclic Voltammetry	28
CHAPTER II	Literature Review
2.1 Development History of Battery	30
2.2 Modification of LTO	32
2.3 Atomic Doping of $\text{Li}_4\text{Ti}_5\text{O}_{12}$	32
2.4 Transition Metal Doping	33
2.5 Doped by Metal in the Main Group	37
2.6 Doped by Non-metal in Carbon Group	38
2.7 Purpose of the Research Work	40
CHAPTER III	Experimental
3.1 Chemicals	41
3.2 Characterization Equipment	42
3.3 Preparation Method for LTO Based Anode Material	42
3.4 Fabrication of Electrode	44
CHAPTER IV	Results and Discussion
4.1 FTIR Spectra Analyses of Prepared LTO Based Materials	45

4.2	XRD Spectra Analyses of Prepared LTO Based Materials	49
4.3	SEM Analysis	56
4.4	Prepared LTO Based Materials Electrochemical Works	58
CHAPTER V	Conclusions	60
References		61

List of Tables

Table No.	Description	Page
1.1	Crystal Structure data for spinel-LTO and rock-salt LTO	8
1.2	Properties of LTO synthesized by different methods in terms of particle size and shape, electrochemical performance	19
2.1	History of electrochemical cell development	30
2.2	The properties of LTO doped by transitional metal	33
2.3	Comparison of discharge capacity and cycling stability of the LTO and doped Cu- LTO anode materials	36
2.4	Doping properties of LTO by metal in the main group	37
3.1	List of all chemicals	41
3.2	Information of the instruments used in this experiment	42
4.1	FTIR data analysis for LTO	48
4.2	List of important peaks of the prepared $\text{Li}_4\text{Ti}_5\text{O}_{12}$	52
4.3	List of important peaks of the prepared $\text{Li}_4\text{Ti}_{4.9}\text{Cu}_{0.05}\text{Zn}_{0.05}\text{O}_{12}$	53
4.4	List of important peaks of the prepared $\text{Li}_{3.9}\text{Ti}_5\text{Cu}_{0.05}\text{Zn}_{0.05}\text{O}_{12}$	54
4.5	List of important peaks of the prepared $\text{Li}_{3.9}\text{Ti}_{4.9}\text{Cu}_{0.1}\text{Zn}_{0.1}\text{O}_{12}$	55

List of Figures

Figure No.	Description	Page
1.1	A simple schematic presentation of storage and charge/discharge mechanism in a conventional lithium ion battery comprised of a metal oxide cathode vs graphitic anode. Charge is indicated by green arrows and discharge is indicated by red arrows for the electrons and the ions	2
1.2	Unit cell of $\text{Li}_4\text{Ti}_5\text{O}_{12}$ ($[\text{Li}]_{8a}[\text{Li}_{1/3}\text{Ti}_{5/3}]_{16d}\text{O}_4$) (a) and $\text{Li}_7\text{Ti}_5\text{O}_{12}$ ($[\text{Li}_2]_{16c}[\text{Li}_{1/3}\text{Ti}_{5/3}]_{16d}\text{O}_4$) (b). The stable frame of $[\text{Li}_{1/3}\text{Ti}_{5/3}]_{16d}\text{O}_4$ is shown as an octahedron and $[\text{Li}]_{8a}$ is centered in a tetrahedron	7
1.3	Crystal structures of $\text{Li}_4\text{Ti}_5\text{O}_{12}$ and $\text{Li}_7\text{Ti}_5\text{O}_{12}$	9
1.4	Illustration of the charging/discharging process of LTO	10
1.5	General working principle of the charging/discharging process of a rechargeable lithium-ion battery	11
1.6	FTIR Machine	22
1.7	XRD Machine	24
1.8	Schematics of Bragg's Law for the scattering of X-rays at periodic crystal lattice planes	24
1.9	Picture of a scanning electron microscope machine	26
1.10	Working procedure of SEM	27
1.11	Schematic diagram of a SEM	28
1.12	Cyclic Voltammogram response for a reversible redox couple	29
3.1	Pictorial view of the synthesized LTO based composite materials	44
4.1	FTIR spectrum of pure $\text{Li}_4\text{Ti}_5\text{O}_{12}$	46
4.2	FTIR spectrum of $\text{Li}_4\text{Ti}_{4.9}\text{Cu}_{0.05}\text{Zn}_{0.05}\text{O}_{12}$	47
4.3	FTIR spectrum of $\text{Li}_{3.9}\text{Ti}_5\text{Cu}_{0.05}\text{Zn}_{0.05}\text{O}_{12}$	47
4.4	FTIR spectrum of $\text{Li}_{3.9}\text{Ti}_{4.9}\text{Cu}_{0.1}\text{Zn}_{0.1}\text{O}_{12}$	48

4.5	Crystal structure of spinel LTO with Fd3m space group. Black: Li ⁺ . Octahedron with 16d and 16c site share common edge 16d and 16c site share common faces with tetrahedron 48f. Lithium can transport through 8a site to 16c site and vice versa	49
4.6	(a) Li ₄ Ti ₅ O ₁₂ spinel structure type. Blue tetrahedra represent lithium and green octahedra represent disordered lithium and titanium (b) Li ₇ Ti ₅ O ₁₂ rock salt. Blue octahedra represent lithium and green octahedra represent disordered lithium and titanium	50
4.7	XRD spectrum of pure Li ₄ Ti ₅ O ₁₂	52
4.8	XRD spectrum of Zn & Cu co-doped Li ₄ Ti _{4.9} Cu _{0.05} Zn _{0.05} O ₁₂	53
4.9	XRD spectrum of Zn & Cu co-doped Li _{3.9} Ti ₅ Cu _{0.05} Zn _{0.05} O ₁₂	54
4.10	XRD spectrum of Zn & Cu co-doped Li _{3.9} Ti _{4.9} Cu _{0.1} Zn _{0.1} O ₁₂	55
4.11	SEM image of pure Li ₄ Ti ₅ O ₁₂ at different magnifications	56
4.12	SEM image of Cu and Zn doped Li ₄ Ti _{4.9} Cu _{0.05} Zn _{0.05} O ₁₂ (LTO) at different magnifications	57
4.13	SEM image of Cu and Zn doped Li _{3.9} Ti ₅ Cu _{0.05} Zn _{0.05} O ₁₂ (LTO) at different magnifications	57
4.14	SEM image of Cu and Zn doped Li _{3.9} Ti _{4.9} Cu _{0.1} Zn _{0.1} O ₁₂ (LTO) at different magnifications	58
4.15	Fabricate cell	58
4.16	Cyclovoltammogram of the fabricated cell	59

List of Symbols and Abbreviations

LIB	Li-ion battery
LTO	Lithium Titanium Oxide
EC	Ethylene Carbonate
PC	Propylene Carbonate
DMC	Dimethyl Carbonate
DEC	Diethyl Carbonate
EC	Ethylene Carbonate
EMC	Ethyl Methyl Carbonate
LiPF ₆	Lithium Hexafluorophosphate
PVDF	Polyvinylidene Fluoride
NMP	N-methylpyrrolidine
TEA	Triethanol Amine
XRD	X-ray Diffraction
SEM	Scanning Electron Microscopy
FTIR	Fourier-Transform Infrared Spectroscopy
SE	Scattered Electron
PVDF	Polyvinylidene Fluoride
JCPDS	Joint Committee of Powder Diffraction Standards
λ	Wavelength
θ	Angle Between incident X-ray beam and crystallographic planes
n	Order of the diffraction peak
d	Distance
h, l & k	Miller Indices
a	Lattice Parameter

Chapter – I

Introduction

1.1 General

The ever increasing demand of the portable electronics industry, the electric vehicle market and storage for alternative energy sources has put energy storage devices at the lead of technological investigations [1]. Although there may be many ways to store the uneven power that is from different energy resources, the demands and route of progress of the moveable electronic and electric vehicle industries relies profoundly on electrochemical storage devices, both batteries and super capacitors. This essential on electrochemical storage devices and the necessity to shift toward higher energy density and low mass devices has specifically intensive research attention on solid state devices e.g., lithium ion batteries, Nickel ion batteries etc.

1.2 Lithium Ion Batteries

Li-ion battery (LIB) is a type of rechargeable battery, first suggested by chemist M Stanley Whittingham at Exxon in the 1970s [2]. Whittingham used titanium (IV) sulfide and lithium metal as the electrodes. However, this rechargeable lithium battery could never be completed practical. But efforts to create re-chargeable LIBs followed in the 1980s, although these failed due to the intrinsic changeability of the packs along with the resulting safety concerns. Next important analysis on re-chargeable LIB packs throughout the 1980s and finally SONY manufactured and sold the initial Li-ion battery for commercial consumption in 1991. Since then a vast development occurred in storage energy sector in the name of LIBs. People are using it frequently in mobile phones, laptops and tablets, cameras, handheld game consoles, torches, cordless drills, sanders, saws, multiplicity of garden equipment, rechargeable cars, hybrid vehicles, electric motorcycles, scooters, electric bicycles, electric wheelchairs, model aircraft etc. and when they required. It has vast uses and advantages such as, relatively higher energy density, capability for still superior capacities, quite low self-discharge, minimal upkeep, no irregular discharge is required, no memory etc.

In LIB lithium ions transfer from the negative electrode to the positive electrode during discharge and back after charging (Figure 1.1). Lithium ion electrodes are conventionally intercalation materials where the lithium ions present in between the layers and spaces in the lattice structures of the host material. A material's propensity to accept lithium ions inside its structure defines its storage capacity and capability as an electrode material.

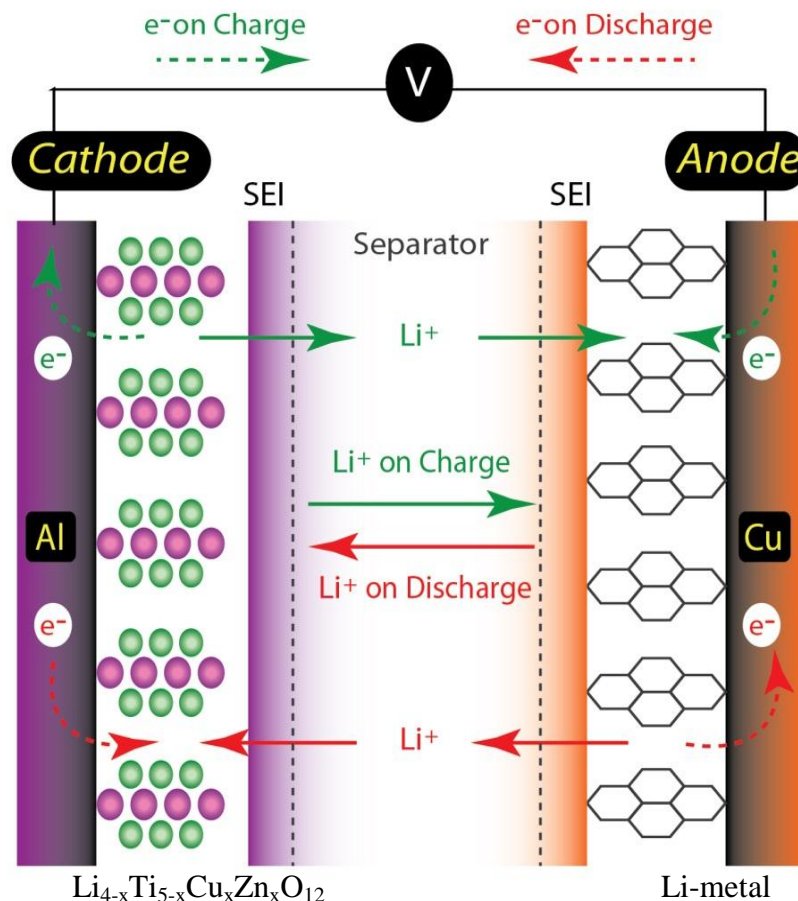


Figure 1.1: A simple schematic presentation of storage and charge/discharge mechanism in a conventional lithium ion battery comprised of a metal oxide cathode vs graphitic anode. Charge is indicated by green arrows and discharge is indicated by red arrows for the electrons and the ions [3]

1.3 Lithium Ion Battery Components

The three key functional elements of lithium ion batteries are cathode, anode, and electrolyte. The cathode is the positive electrode that is condensed through the reaction, and the lithium ions are deposited within the cathode when the cell is discharged. Transition metal oxides have traditionally been the material of special for

cathodes used in high energy density applications. Yet there is soft motivated attention to identify and improve anode and cathode materials that growth the energy density further, while enlightening rate capability and security. There are numerous key abilities of any good cathode material, namely, the cathode must agree for noteworthy and unchanging reversible intercalation of lithium ions; exhibit low electron energy and site energy for Li-ions; electrode potential should fluctuate little with Li^+ content; determine fast diffusion of electrons and Li^+ ; stable over operating voltage range; low cost; lack of harmfulness; comfort of preparation and reproducibility; and promising interface designed at contact with electrolyte [4].

Different cathode materials such as LiCoPO_4 , LiMnPO_4 , LiCoO_2 , LiNiO_2 , Li have been inspected to report many of these contributing factors, each offering distinctive benefits, but also exposing possible drawbacks. Manganese oxide chemistries, LiNiO_2 , LiMnO_2 , and spinel LiMn_2O_4 have their individual advantages in safety and cost; though the lower capacity, as matched to the lithiated cobalt-oxide chemistry, is one disadvantage [5]. Vanadium oxide chemistries can occur in a variety of phases and have been used as electrode materials also. Though they have high capacities, their voltages are usually lower than the transition metal oxides, manufacture them appropriate for only certain uses [4]. Moreover, novel phosphate chemistries have been established and initiate appropriate for applications demanding advanced power capabilities; LiMnPO_4 and LiCoPO_4 exhibit higher open circuit voltages over metal oxide chemistries, in the range of 4.1 – 4.9 V [5]. Specially, LiFePO_4 meets many of the measures for actual cathode materials, exactly its capability to cycle well at high current rates, its durability against overcharge assembly it a much harmless material, and its cheap manufacture costs.

The anode is the negative electrode that is oxidized during the battery discharge reaction and where the lithium ions are stored when the cell is fully charged. The evolution of lithium ion batteries from lithium batteries came about primarily from the shift in anode material toward carbonaceous or lithium alloy materials and away from pure lithium metal. The low voltage versus lithium of a variety of carbonaceous materials led to the investigation and use of graphite, carbon fibers and meso carbon micro beads as the active material in commercial anodes. Graphite materials tend to be efficient intercalation materials, and the mechanism of storage that results in the stoichiometry of LiC_6 and a theoretical storage capacity of 372 mA.h.g^{-1} in these

materials is well understood [4]. Additionally, carbon anodes have been an excellent initial choice because of their high storage capacity, low cost, long cycle life, small volume change of $< 9\%$ upon lithiation, and negative reduction-oxidation potential versus the cathode. In regards to lithium alloys, Group III, IV, and V elements have been studied because of their capability to store lithium at low voltages LiAl and LiSn systems were initially examined and followed shortly by silicon because it confirms the highest possible gravimetric capacity over $4000 \text{ mA}\cdot\text{h}\cdot\text{g}^{-1}$ [6].

In spite of the potential for high voltage batteries and huge gravimetric capacities with these anode materials there is inadequate large scale commercial usage of these alloy materials. The primary cause is because a large volumetric expansion is related with each of these elements upon lithiation oscillating from 100 to 400 % depending on the specific material. With an extension that great during lithiation, the electrode easily cracks and delaminates from the current collector interpreting the battery ineffective.

Current investigations into overcoming this problem have led to a multiplicity of other anode materials for lithium ion battery. Recently, spinel lithium titanium (LTO) have involved more and more consideration as a potential anode material for lithium ion batteries, attributes to its outstanding structural stability (no structural or volume change during Li insertion and extraction) and no risk of lithium plating during the fast charge/discharge rate with 1.55 V vs Li^+/Li reduction potential of LTO [7]. In evaluation to carbonaceous anode, spinel lithium titanium LTO has well electrochemical performance and higher safety. It is cheaper and easier to be manufactured correlated with alloy-based anode in lithium ion batteries. Researchers have specified that LTO would be a good alternative for graphite in high-safety LIBs. To our best knowledge, it was studied as early as in 1984 by Edwards et al, [8] then planned to be cathode in 1989 by Colbow and coworkers. In 2005, it became firstly commercialized by Altairnano Corporation, who substituted traditional graphite materials for anode material.

The electrolyte and separator combination within a lithium ion battery is a key component which requires some important considerations for optimal battery performance. The ionic conductivity of the electrolyte should be high to reduce internal cell resistance. In addition the permanence of the electrolyte is an important factor in two ways; a) a high chemical stability stops decomposition of the electrolyte

on highly reducing anodes or oxidizing cathodes, and b) a large voltage window of electrochemical stability as determined by the voltage difference between the cathode and anode (typically > 4 V). Furthermore a low melting point and a high boiling point can deliver sufficient conductivity and improve the battery safety by avoiding solidification of the electrolyte and explosive reactions at high temperatures. Non-toxicity of the electrolyte in terms of environmental concerns and ease of handling permit for the scale-up usage of a suitable material, and lastly, an electrolyte at an inexpensive cost as matched to other power sources will aid in its marketable capability [9].

While a host of lithium salts exist, most exhibit detrimental characteristics for battery performance (i.e. toxic side chemical reactions in the solvents); lithium hexafluoro phosphate (LiPF_6), being the least damaging, is widely used in electrolyte chemistries. Lithium bis (oxalato) borate is another potentially effective salt, and along with LiPF_6 , used in concentrations of 0.4 to 1M [10]. LiPF_6 works well in a voltage range of 0 – 4.5 V because of its high electrochemical stability, but its thermal stability raises concerns in addition to its extreme sensitivity to water which can lead to the formation of hydrofluoric acid within the cell causing performance degradation.

Organic carbonates are suitable and have been widely investigated in lithium ion batteries; ethylene carbonate (EC), propylene carbonate (PC), dimethyl carbonate (DMC), diethyl carbonate (DEC), ethyl methyl carbonate (EMC), and more recently γ -butyrolactone (GBL) are commonly used electrolyte solvents, most often found in binary or ternary solvent systems [11]. Non-aqueous electrolytes generally are used non-coordinating anion salts such as lithium hexafluorophosphate (LiPF_6), lithium perchlorate (LiClO_4), lithium hexafluoroarsenate monohydrate (LiAsF_6), lithium tetrafluoroborate (LiBF_4), and lithium triflate (LiCF_3SO_3). Combinations of cyclic and linear carbonates demonstrate enhanced performance, particularly at lower temperatures, over single solvent electrolytes; this improved performance is attributed to the decrease in viscosity as a linear carbonate is combined with a cyclic one.

1.4 Opportunities in Lithium Ion Batteries

The demand for smaller storage devices continues to grow and there are ongoing investigations into developing superior materials to meet the industries demands of small and high performance devices. The development of batteries has progressed

slowly because of many obstacles posed by cost, safety, and environmental compatibility. The potential to improve battery performance lies in several areas of battery development, with active materials and electrolyte chemistries being two with the biggest opportunities for growth. Because each of these fields is enormous in their breadth, a detailed and thorough investigation of any one specific area necessitates limiting the scope of study. This work will focus on the development from synthesis to device testing of high storage capacity nanomaterial for their use in lithium ion battery anodes to increase the energy and power density of the anode and in turn the full cell.

1.5 Motivation for LTO as Anode Material

The commercial anode material of LIBs is graphite. Graphite can accommodate Li^+ ions to form LiC_6 and provides a specific capacity of 372 mA.h.g^{-1} . The intercalation reaction of Li^+ ions into graphite occurs at the potential of around $0.5\sim 0.6 \text{ V vs Li}^+/\text{Li}$. Lithium deposition, however, may take place to form lithium dendrites on graphite at such low potential. Lithium dendrites can penetrate the separator resulting in a short circuit. The electrolytes with special additives can be decomposed to form a solid electrolyte interface (SEI) film and this SEI film on the surface of graphite can prevent the formation of lithium dendrites. On the other hand, the stability of the SEI film and undesired structural changes in graphite (e.g., exploitation or non-active sites) during the charging and discharging process are detrimental to safety and lifetime of LIBs [12]. Therefore seeking an alternative anode material has attracted more and more attention.

A large number of candidates for anode materials have been extensively studied over the past two decades. In brief, these candidates can be divided into several categories: alloy reaction materials such as Si, Sn, Sb and Ge; conversion reaction materials such as iron oxide, nickel oxide, and cobalt oxide; and intercalation reaction materials such as lithium titanate spinel (LTO) and anatase (TiO_2). Alloy anode materials have an ultra-high specific capacity, which can be up to 10 times higher than that of graphite. On the other hand, the volume of alloy anode materials expands 2 to 3 times after the full lithiation, for instance, 3.2-fold expansion for Si and 2.6-fold expansion for Sn. The considerable volume change during lithiation/delithiation reaction will bring about a pulverization and isolation of active materials in the electrode, leading to a poor cycle stability [13]. Transition metal oxides such Fe_2O_3 , CuO and CoO can

undergo reversible reduction in the presence of Li^+ ions, delivering 2 or 3 times higher specific capacity than that of graphite [14]. Metal sulfides, phosphides and fluorides have been proven to be able to undergo such reaction as well. The low Coulombic efficiency and cycle stability derived from the irreversible phase transformation at the reduction process impede their application. Further the other promising candidates for anode materials are intercalation reaction materials. More and more attention have been paid to the Ti-based materials such as LTO and TiO_2 (e.g., anatase, rutile, brookite, TiO_2 -b and even amorphous), attributed to their structural stability during the intercalation reaction [15].

1.6 Structure of LTO

LTO was first reported as an anode material for LIBs in 1994, and since then numerous studies have been carried out in order to learn its electrochemical and structural properties [16]. Li^+ ions can be reversibly inserted into and extracted from LTO at a potential of 1.55 V vs Li^+/Li . The high intercalation potential of LTO prevents lithium deposition and electrolyte decomposition, which is crucial for electrode durability and safety. The spinel structure of $\text{Li}_4\text{Ti}_5\text{O}_{12}$ ($\text{Fd}\bar{3}\text{m}$) comprises eight formula units of $(\text{Li})^{8a}[\text{Li}_{1/3}\text{Ti}_{5/3}]^{16d}\text{O}_4^{32e}$ per unit cell, in which Li^+ entirely occupies 8 tetrahedral (a) sites, while the 16 octahedral (d) sites are occupied by one-third Li^+ and five-third Ti^{4+} (seeing Figure 1.2). The remaining oxygen ions on 32e sites form a cubic close-packed structure. Intriguingly, during the lithiation,

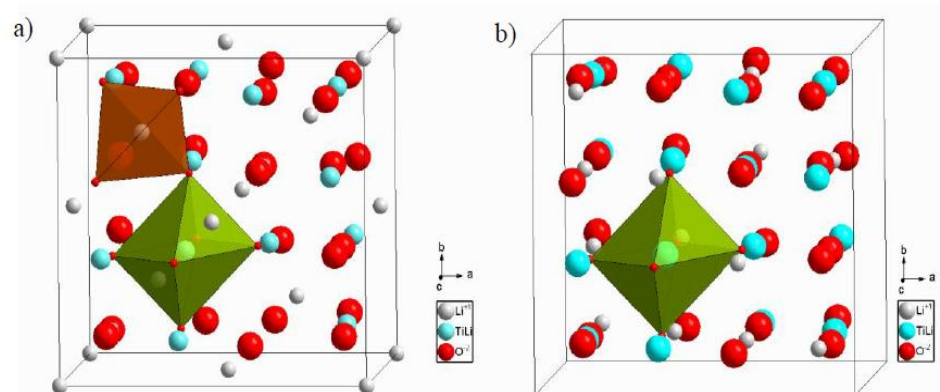
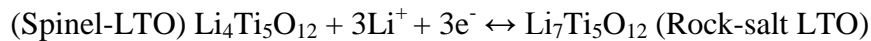


Figure 1.2 Unit cell of $\text{Li}_4\text{Ti}_5\text{O}_{12}$ ($[\text{Li}]_{8a}[\text{Li}_{1/3}\text{Ti}_{5/3}]_{16d}\text{O}_4$) (a) and $\text{Li}_7\text{Ti}_5\text{O}_{12}$ ($[\text{Li}]_{16c}[\text{Li}_{1/3}\text{Ti}_{5/3}]_{16d}\text{O}_4$) (b). The stable frame of $[\text{Li}_{1/3}\text{Ti}_{5/3}]_{16d}\text{O}_4$ is shown as an octahedron and $[\text{Li}]_{8a}$ is centered in a tetrahedron.

the $\text{Li}_4\text{Ti}_5\text{O}_{12}$ structure undergoes a change to $[(\text{Li})_{1-x}^{8a}[\text{Li}]_{2x}^{16c}[\text{Li}_{1/3}\text{Ti}_{5/3}]^{16d}\text{O}_4^{32e}]$, which is accompanied by a minor volume expansion of $\sim 0.2\%$ due to the migration of Li^+ ions from tetrahedral (a) sites toward octahedral (c) sites [17]. The advantage of LTO derived from structural stability as “zero strain” material enables safe operation, high rate capacity and excellent cyclability.

1.7 Phase Transition Behavior of $\text{Li}_4\text{Ti}_5\text{O}_{12}$ and $\text{Li}_7\text{Ti}_5\text{O}_{12}$

Twenty years ago, Ohzuku and co-authors[18] reported that the charge/discharge curve for $\text{Li}_4\text{Ti}_5\text{O}_{12}$ (LTO) electrode as anode is characterized by a very flat and extended voltage plateau at around 1.55 V, which is a typical characteristic of phase transition between a Li-rich phase ($\text{Li}_7\text{Ti}_5\text{O}_{12}$, rock-salt LTO) and a Li-poor phase ($\text{Li}_4\text{Ti}_5\text{O}_{12}$, spinel-LTO). Although substantial chemical changes occur during conversion between the two phases, a negligible volume change of 0.2 - 0.3% occurs between two phase changes accompanied by a change of the lattice from 0.8364 nm to 0.8353 nm, and as a result it is called the “zero-strain insertion materials”, which indicating that it is an excellent material with exceptional reversibility performance as anode material for LIBs. As well investigated and discussed [19] three Ti^{4+} ions are reduced to Ti^{3+} ions during the two-phase transition from spinel-LTO into rock-salt LTO. The corresponding electrochemical reaction can be briefly described during the lithium insertion and extraction processes as:



Two types of LTO crystallographic data is summarized in Table 1.1 [20]. It is

Table 1.1: Crystal Structure data for spinel-LTO and rock-salt LTO [20]

Materials Atom Wyckoff (space group) Site			Cell parameter			Occupancy
			x	Y	Z	
Spinel-LTO (Fd3m)	Li1	8a	0.125	0.125	0.125	1.0
	Li2	16d	0.5	0.5	0.5	0.01667
	Ti	16d	0.5	0.5	0.5	0.8333
	O	32e	0.2625(1)	0.2625(1)	0.2625(1)	1.0
Rock-salt LTO	Li1	8a	0	0	0	1.0
	Li2	16d	0.5	0.5	0.5	0.1667

(Fd3m)	Ti	16d	0.5	0.5	0.5	0.8333
	O	32e	0.2576(3)	0.2576(3)	0.2576(3)	1.0

apparent that spinel-LTO and rock-salt LTO has very similar crystallographic parameters, which demonstrate the structural stability during the charge/discharge processing when LTO electrode is applied as anode.

Figure 1.3: shows the structure of spinel LTO crystallized in the space group (Fd3m). [18, 21] Lithium ions and titanium ions randomly occupy the octahedral (16d) sites, while the tetrahedral (8a) sites are occupied by lithium. As three lithium ions insert into spinel LTO and occupy the octahedral (16c) positions, the tetrahedral lithium ions of $\text{Li}_4\text{Ti}_5\text{O}_{12}$ are shifted to the octahedral (16c) sites and LTO crystallizes in the space group with ordered rock-salt structure, as shown in Figure 1.1. In contrast to spinel structure, the octahedral 16d positions are still occupied by lithium ions and titanium ions, whereas the tetrahedral (8a) sites in $\text{Li}_7\text{Ti}_5\text{O}_{12}$ are free. They are described by the cubic space group and have very similar lattice parameters ($a = 0.83595$ and 0.83538 nm, respectively) [18, 21].

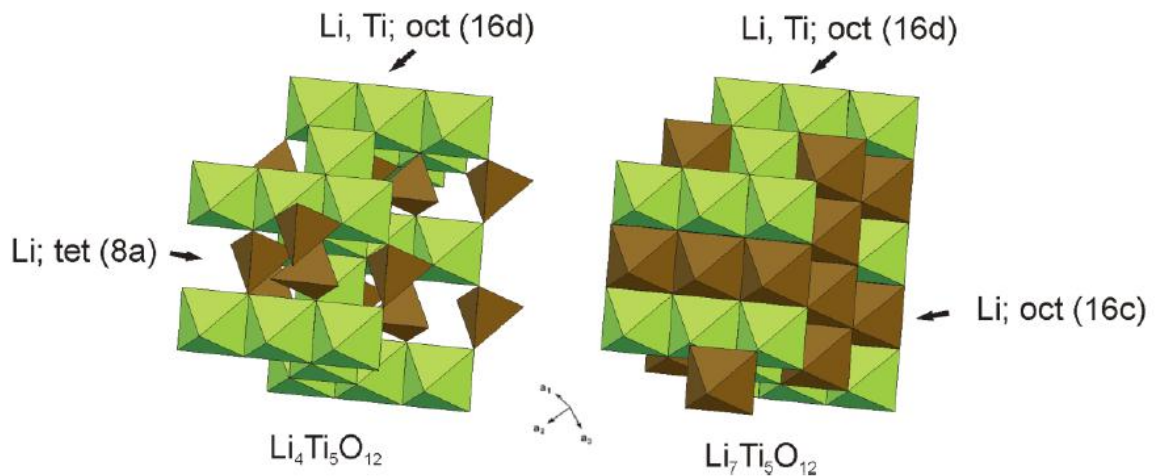


Figure 1.3: Crystal structures of $\text{Li}_4\text{Ti}_5\text{O}_{12}$ and $\text{Li}_7\text{Ti}_5\text{O}_{12}$ [21]

Spinel LTO is a good lithium ion conductor (10^{-6} cm^2/s) and very poor electronic conductor (10^{-8} S/cm) [22] because of the existence of available free octahedral (16c) sites in its lattice and the oxidation state of Ti^{4+} . On the other hand, $\text{Li}_7\text{Ti}_5\text{O}_{12}$ is a good electronic conductor (10^{-2} S/cm) and poor lithium ion conductor because Ti^{3+} ions occupy 60% of all the oxidation state of Ti and the full 16c octahedral sites in the lattice are occupied by Li^+ ions.

The typical core-shell model has described a reasonable two-phase transition process [21, 22] as illustrated in Figure 1.4, when the lithium intercalation (discharge) proceeds, the spinel-LTO on the surface of the particle is reduced and transformed to a rock-salt-LTO structure. Then, the shell with rock-salt structure is formed and becomes increasingly thicker with the increasing depth of lithium insertion. Simultaneously, the core with spinel structure shrinks. At the end of discharging process, the entire particle becomes rock-salt LTO. Vice versa, the particle transforms from rock-salt into spinel phase during the charging (lithium extraction) process.

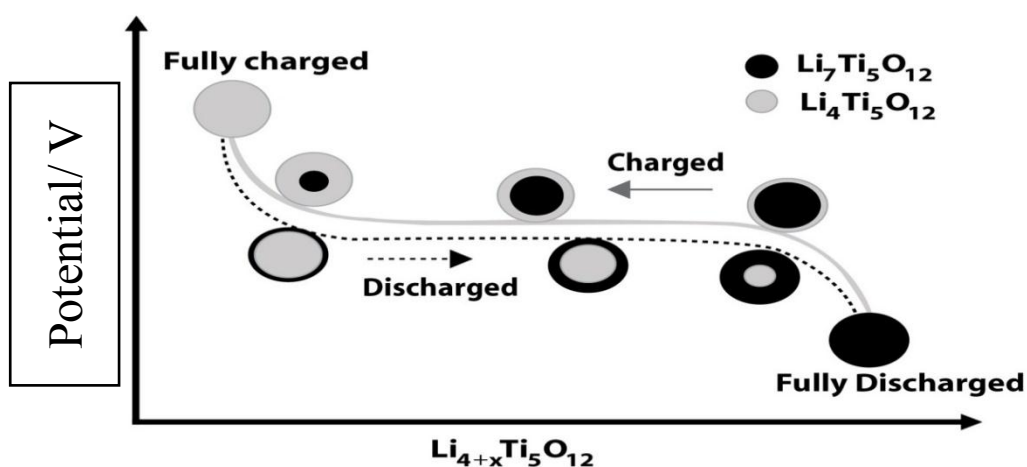


Figure 1.4 Illustration of the charging/discharging process of LTO [22]

1.8 Why Rechargeable Li-Ion Battery (LIB)?

Depending on their rechargeable capability, electrochemical batteries (or cells) are identified as primary or secondary batteries. Primary batteries can only be used once, and not capable of being recharged electrically. For example, alkaline-manganese dioxide battery and zinc-carbon battery are typical primary batteries. The batteries with rechargeable capability are classified as secondary batteries. Major secondary batteries include rechargeable lead-acid, Ni-Cd, Ni-MH (M-metal) and lithium ion batteries [23]. Compared with other secondary batteries, rechargeable lithium ion batteries show excellent electrochemical performance, which leads to their predominant position in the present battery industry.

So far, among various existing technologies (e.g., lead-acid, nickel-cadmium, metal-lithium), rechargeable lithium-ion batteries (LIBs) have the advantage of high voltage,

long cycling life, high power, high reliability and design flexibility (see Figure 1.4) [24] the significance and popularity of the rechargeable lithium-ion batteries are definitely resulted from its unique advantages offered over other secondary batteries:

- Lighter than other rechargeable batteries for a given capacity
- Li-ion chemistry delivers a high open-circuit voltage
- Low self-discharge rate (about 1.5% per month)
- Do not suffer from battery memory effect
- Environmental benefits in rechargeable and reduced toxic landfill

1.9 Working Principle of Li-Ion Battery

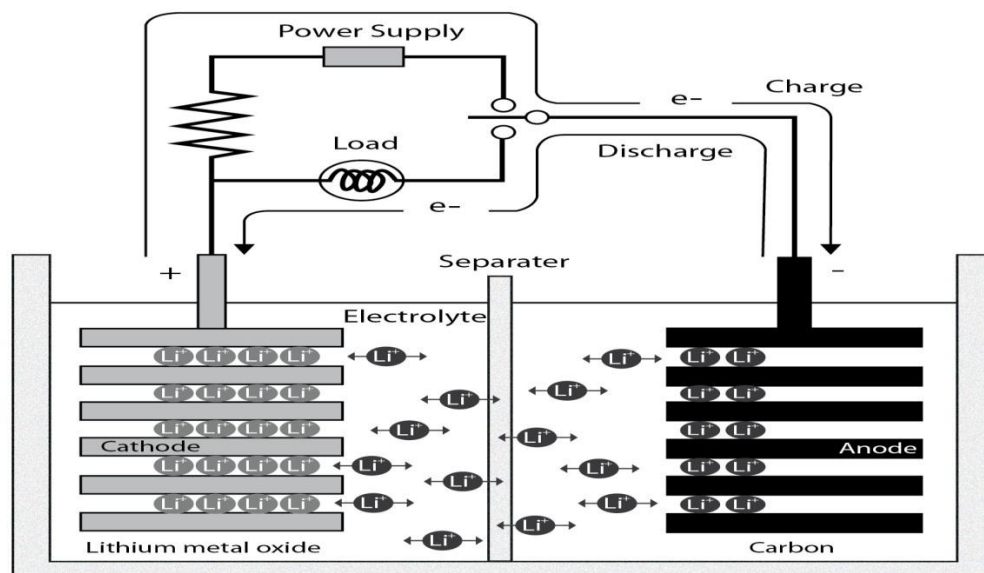


Figure 1.5. General working principle of the charging/discharging process of a rechargeable lithium-ion battery [25]

In general, there are five components that establish a lithium-ion cell. These components are two electrodes, electrolyte, and two current collectors. The main function of the electrodes is to be reduced or oxidized over a potential range measured in volts (V). The electrolyte serves as an ionic conductor between the electrodes and must be electronically insulating. The current collectors are an electrically conducting material, usually a metal that are directly in contact with each electrode. The current collectors are attached to each other by an external circuit (see Figure 1.5) [26]. A

lithium-ion battery exhibits the electrochemical cell functions because of the potential difference between the two electrodes. It is energetically favorable for the two electrodes to come towards an equilibrium potential that is lower than the initial open-circuit cell potential where they are stable. Equilibrium between the electrodes is achieved by the oxidation of one electrode and the reduction of the other electrode. The electrode that is reduced is called the cathode, while the electrode that is oxidized is called the anode. These reactions are accomplished by two distinct paths for ions and electrons. The electrons travel through the external circuit from the anode to the cathode. At the same time, the ions travel in the same direction as the electrons between the two electrodes through the electrolyte. This completes the redox reaction of the two electrodes, as showed clearly in Figure 1.5.

Usually, the basic working principle of lithium-ion batteries is based on lithium ion (Li^+) reversible de-intercalation and intercalation processes between two electrodes [27]. As a result, during charge/discharge, Li^+ ions movement between the anode and the cathode, permitting the conversion of chemical energy into electrical energy and the storage of electrochemical energy within the battery. Now, the electrolyte should be ionically conducting and electronically insulating, however the actual properties of the electrolyte are much more complex. During the first cycle, a solid–electrolyte-interphase (SEI) layer will be formed on the surface of electrodes due to the decomposition of organic electrolyte [27]. The typical electrochemical reactions involved in a typical LIB cell are described in Figure 1.5.

The charge/discharge mechanism of a LIB is also known as a “rocking chair” concept as Li^+ ions “rock” back and forth between anode and cathode [28]. As is shown in Figure 1.5, lithium ions are shuttled between anode and cathode through the electrolyte during the charging and discharging processes. Lithium ions de-intercalate from the cathode into the electrolyte during the charging process under an applied current. Instantaneously, an equivalent amount of lithium ions from the electrolyte introduce into the anode. The reverse reaction proceeds spontaneously when the battery is discharged. On both of the charging and discharging process, charge compensation is provided by the external circuit supply.

A LIB essentially consists of a cathode, an anode, electrolyte and a separator. The cathode materials are commonly Li-containing transition metal oxides with a layered

structure (such as lithium cobalt oxide) or tunnel-structured materials (such as lithium manganese oxide). The anode materials contain insertion-type materials (such as graphite, TiO_2 , etc.), conversion-type materials (such as iron oxides, nickel oxides, cobalt oxides, etc.) and alloying-type materials (such as Si, Sn etc.). The electrolyte is hypothetical to be a good ionic conductor and electronic insulator. Most of the electrolytes are founded on the solution of inorganic lithium salts liquefied in a mixture of two or more organic solvents. The purpose of the separator is to prevent short circuit between the two electrodes and to provide abundant channels for transportation of Li ion during the process of charging/discharging.

1.10 Cathode

Cathode materials are typically Li-containing oxides of transition metals with layer structure, which undergo oxidation reaction to higher valences when lithium is removed. While oxidation of the transition metal can maintain charge neutrality in the compound, large compositional changes often lead to phase changes, so crystal structures that are stable over wide ranges of composition must be used. This structural stability is a particular challenge during charging when most (ideally all) of the lithium is removed from the cathode. During discharge lithium is inserted into the cathode material and electrons from the anode reduce the transition metal ions in the cathode to a lower valence. The key requirements for a successful cathode material in a rechargeable LIB are as follows [29]:

- 1) The material contains a readily reducible/oxidizable ion, for example a transition metal
- 2) The material reacts with lithium in a reversible manner
- 3) The material reacts with lithium with a high free energy of reaction
- 4) The material reacts with lithium very rapidly during both insertion and extraction processes
- 5) The material is supposed to be a good electronic conductor, preferably a metal
- 6) The material should be stable. For example, there won't be structure changing or degrading if over-discharging or over-charging takes place
- 7) The material should be less expensive
- 8) The material is better to be environmentally friendly

During the early age of LIBs, metal chalcogenides (e.g., TiS_2 and MoS_2) and manganese or vanadium oxides were chosen as the cathode materials to pair with the metallic Li or the graphite anode. After several decades development and the increasing requirement of high-performance electrode material from large-scale energy storage, the main focus on the cathode materials for LIBs has been devoted to layered, structured hexagonal LiCoO_2 , spinel LiMn_2O_4 , olivine LiFePO_4 , and their derivatives.

1.10.1 Layered Structured Cathode

There are three basic layered cathode materials: LiCoO_2 , LiNiO_2 and LiMnO_2 . LiCoO_2 has been and is still widely used in commercialized LIBs since it's first patented as a lithium intercalation cathode material in 1980 by good enough and its first appearance in the commercial LIBs by SONY in 1991. It possesses the advantages of large theoretical capacity ($274 \text{ mAh}\cdot\text{g}^{-1}$, calculated based on extraction of 1 mole of Li^+ from LiCoO_2) and high working voltage ($>3.4\text{V}$). The cathode undergoes serious phase transformation between hexagonal and monoclinic when the cathode charged above 4.2 V. Since this phase transformation leads deterioration of cycling performance, practical capacity is restricted as half of theoretical capacity. Although the LiCoO_2 cathode dominates the LIB market, there is a limited availability of cobalt, which makes the cost of a single battery expensive. This price limits its application only in the area of small cells of portable electrical devices, such as those used in computers, cell phones, and cameras [29].

Lithium nickel oxide, LiNiO_2 , due to the configuration of low spin $\text{Ni}^{3+}:t_{2g}^6e_g^1$, electrons are removed only from the e.g. band that barely touches the top of the $\text{O}^{2-}:2p$ band, thus most of the lithium can be extracted from LiNiO_2 prior to the oxygen loss and a high capacity of around $200 \text{ mA}\cdot\text{h}\cdot\text{g}^{-1}$ is generated [30]. LiNiO_2 has the same structure with lithium cobalt oxide but has not been pursued in the pure state as a battery cathode for a variety of reasons, even though nickel is less expensive than cobalt. First, it is not clear that stoichiometric LiNiO_2 exists. Most reports suggest excess nickel as in $\text{Li}_{1-y}\text{Ni}_{1+y}\text{O}_2$; thus, nickel is always found in the lithium layer, which pins the NiO_2 layers together, thereby reducing the lithium diffusion coefficient and the power capability of the electrode. Second, compounds with low lithium

contents appear to be unstable due to the high effective equilibrium oxygen partial pressure, so that such cells are inherently unstable and therefore dangerous in contact with organic solvents [29]. There are two structures of LiMnO_2 , the layered structure and the orthorhombic phase. The layered structure is thermodynamically more stable. The layered LiMnO_2 can be synthesized using the soft chemical method such as ion-exchange from the sodium analogue NaMnO_2 [31]. Generally speaking, the manganese based material has advantages of low price and low toxicity and high initial charge capacity. However the main shortcoming of the layered LiMnO_2 is the crystallographic transformation to more stable spinel structure during electrochemical cycling. Mn^{3+} is a Jahn-Teller ion and the redox reaction between Mn^{3+} and Mn^{4+} will result in local distortion and quick capacity decay [32].

1.10.2 Spinel Structured Cathode

LiMn_2O_4 is an extensively studied cathode material for LIBs. Compared with LiCoO_2 , it possesses the advantages of cheaper price, lower toxicity, and higher rate capability. However, the main drawback of spinel LiMn_2O_4 cathode is drastic capacity fading, especially at high temperatures, and shows a low capacity of around $120 \text{ mAh}\cdot\text{g}^{-1}$ [33]. The dissolution of manganese from the lattice into the electrolyte due to a disproportionation of Mn^{3+} ions into Mn^{2+} and Mn^{4+} plays a vital role for the problem, which is facilitated by trace amount of HF generated in the electrolyte [34].

1.10.3 Olivine Structured Cathode

In 1997, Goodenough and co-workers firstly reported reversible lithium intercalation in the phosphate poly anionic compound of LiFePO_4 . The Olivine-type of LiFePO_4 with a theoretical capacity of $170 \text{ mAh}\cdot\text{g}^{-1}$ has been considered as a promising cathode material for LIBs [35]. The main drawbacks of LiFePO_4 are the poor conductivity resulting from the low Li ion diffusion rate and low electronic conductivity.

1.11 Anode

Anode is the negative electrode of a primary cell and is always associated with oxidation reaction, accompanying with release of electrons to external circuit. In a secondary cell, anode is the negative pole during discharge but the positive pole during charge. The basic requirements for a LIB anode material are that the material should have minimal volume expansion and resulting stress during charge/discharge

process, high electronic conductivity, low irreversible capacity during initial charging or intercalation process, stable under wide operating temperature window in a highly reducing environment, and low specific surface area (typically $< 2 \text{ m}^2/\text{g}$) for optimal performance and safety [36].

1.11.1 Metallic Li Anode

The most elementary anode material for lithium-based batteries is metallic lithium, which has been used for primary batteries since the early 1960s. By possessing the lowest standard potential (-3.05 V vs. a standard hydrogen electrode (SHE)) and the lowest atomic weight (6.94 g/mol specific gravity: $\rho = 0.53 \text{ g/cm}^3$) among all metals, the utilization of metallic lithium as an anode offers the realization of galvanostatic cells having an extremely high capacity ($3820 \text{ mAh}\cdot\text{g}^{-1}$) and energy density ($1470 \text{ W}\cdot\text{kg}^{-1}$) [37]. Consequently, metallic lithium was also considered as the candidate of choice for secondary LIBs. However, lithium metal cells have one severe drawback, namely, inhomogeneous lithium plating, which hinders their commercial development. This uneven deposition of lithium onto the anode surface upon charge results in the formation of so-called dendrites. And the disordered metallic deposit gives rise to a poor Coulombic efficiency, resulting from such a fine Li metal often acts as an active site inducing reductive decomposition of electrolyte components. Part of the deposit may become electrically isolated and shedding may also occur. These dendrites consist of high surface area, highly branched lithium metal structures, which continuously grow, may easily penetrate into the separator and eventually cause internal short, resulting in heat generation and contingent ignition. Hence the hazardous nature of Li has paved way to explore some other safer anode materials, possessing comparably the same electrochemical features as that of metallic lithium.

1.11.2 Carbonaceous Anode

The most commonly used anode material is carbonaceous materials as they possess the advantages of low cost, excellent reversible capacity and long cycling life. Carbon as an insertion anode material was first reported in 1973. Carbonaceous materials have large variations in crystallinity, chemical composition and micro texture depending on their preparation, processing, precursor, thermal and chemical activation treatments. All carbonaceous materials are able to storing lithium ions [38].

Graphitic carbons are characterized by layers of hexagonally arranged carbon atoms in a planar graphene layers. Graphite shows a rather flat potential profile when reversibly hosting Li^+ at potentials below 0.5 V vs. Li/Li^+ . Additionally, it offers a significantly higher specific capacity of 372 mAh/g (corresponding to one lithium per hexagonal carbon ring, i.e. LiC_6) [39]. The volume expansion during lithium intercalation and extraction between the graphene layers is just over 10%, resulting in high reversibility and stable capacity over repeated cycling. However, compared with other alternative anode materials, the theoretical capacity of graphite is far behind to meet the requirement from batteries with high energy density.

1.11.3 Sn and SnO_2 Based Anode

Sn and SnO_2 are promising anode materials with high theoretical capacity. The reversible capacity of Sn is as high as 994 mA.h.g⁻¹ when alloy $\text{Li}_{4.4}\text{Sn}$ forms during lithiation and the theoretical capacity of SnO_2 is 782 mAh.g⁻¹ [40]. However both Sn and SnO_2 suffer from severe volume change during cycling.

One of the most efficient approaches to alleviate the severe volume change and stabilizing the structure is to design nano structured materials, for example, in the form of nano tubes, nanorods, nano wires and hollow structures [40]. Although most of the attempts have been made to synthesize new nanostructures for Sn and SnO_2 , up to now most efforts have been characterized as having technical difficulties or high synthesis costs, and most of them have proved not to be very successful in improving the cycling stability of Sn and SnO_2 -based electrodes [41]. Adding coating materials (such as carbon or other conductive materials) are another method to accommodate volume changes. In addition, the electrical conductivity of the whole electrode could also be enhanced [42].

1.11.4 Lithium Titanate Anode

Lithium titanate (LTO) is another promising anode material with spinel structure for certain applications that require fast charging capability; first reported in 1994 [37]. It has superior high rate performance with very long cycle life. It is being developed for automotive and energy storage applications. Some of the challenges for the LTO-based batteries include lower voltage (2.5 V vs. LiCoO_2), lower capacity, and excellent high-temperature stability [36].

1.11.5 Other Metal Oxide Anode

Apart from SnO₂, other metal oxides, such as Co₃O₄, TiO₂, NiO and Fe₃O₄ have been studied. These metal oxides also suffer from severe aggregation and rapid capacity fading due to dramatic volume expansion and low electrical conductivity [28]. The most commonly studied methods to solve the problems are coating carbon layers on the surface of the metal oxides or dispersing them into carbon matrix.

1.11.6 Graphene-Based Anode

Graphene is a single layer carbon nano sheet consisting of two equivalent sub-lattices of sp² carbon atoms connected by σ bonds. And theoretical calculation showed that graphene possesses a maximum capacity of 740 mA.h.g⁻¹ on the basis of a double-layer adsorption configuration, which is much larger than that of layered graphite. Sato and co-workers [43] used the ⁷Li nuclear magnetic resonance (NMR) technique to study lithium ion transport mechanism in a disordered carbon, and proposed a model of Li₂ covalent molecule configuration that a Li₂ molecule is loosely trapped by two adjacent benzene rings in the carbon. The most saturated Li storage state can be LiC₂ to give a capacity of up to 1116 mA.h.g⁻¹. Both two configurations suggest a higher capacity of graphene anode. Another study showed that graphene and graphite have a similar interaction mode with Li ions after analyzing in situ Raman spectra of lithiation processes in both single and few-layer graphene anodes. However, because of the repulsion forces between Li⁺ at both surfaces of graphene, the amount of adsorbed Li on single-layered graphene is low. Uthaisar and Barone [44] studied the edge effects of Li diffusion in graphene by means of density functional theory and showed that narrower grapheme nano-ribbons, especially with a zigzag morphology, can provide a faster discharge rate owing to the lowering of energy barriers and diffusion lengths. The theories mentioned above can explain the Li storage mechanisms to some extent; however, more work is still needed in the coming future to erase the debate.

1.12 Various Methods of Synthesizing LTO

For synthesis of lithium titanium oxide different methods, including emulsion-gel process, solid state method, hydrothermal or solvothermal method, spray pyrolysis,

composite molten-salt method, template method, reflux method, flux method, mechanochemical synthesis, electro spinning method, solution combustion synthesis, modified solution combustion synthesis, sono chemical method, single step metal organic precursor method, template free hydrothermal process, spray drying process, modified rheological phase method and electro spray pyrolysis method.

Sol-gel method is used for the synthesis of spinel LTO because this technique gives the regular morphology, homogeneity and uniform particle size distribution. So this technique is better than other techniques. Also there are some different kinds of method have been developed for preparing LTO and this techniques exhibit excellent electrochemical performance. LTO synthesis by different methods shows individual characteristic based on particle size and shape, and electrochemical performance, as summarized in Table 1.2.

Table 1.2: Properties of LTO synthesized by different methods in terms of particle size and shape, electrochemical performance

Methods	Particle size (nm)	Shape	Electrochemical performance	Ref.
Solid-state method	70	Spherical	202 mA.h.g ⁻¹ at 0.01-2.5 V	[45]
Sol-gel method	98 – 136	Nanoparticle	Excellent cycliability 272 mA.h.g ⁻¹ - first cycle	[46]
Sol-gel method with different complex agents	76 – 500	Round	170 mA.h.g ⁻¹ - first cycle 150 mA.h.g ⁻¹ - 30 cycles – 0.5 mA·cm ⁻²	[47]
Refluxing method	5 – 400	Spherical	200 mA.h.g ⁻¹ - 0.4 mA·cm ⁻² - 60th cycles	[48]
Heat treatment and an alkali hydrothermal reaction	6 – 11	Nanotubes	~156 mA.h.g ⁻¹ - 0.1 C	[49]
Template-free hydrothermal process	20	Spherical	114 mA.h.g ⁻¹ - 30 C 125 mA.h.g ⁻¹ - 200 cycles - 20 C	[50]

Single step metal organic precursor method	>50	3-D ordered macroporos	167 mA.h.g ⁻¹ - 1st cycle - 0.1 mA. cm ⁻² 149 mA.h.g ⁻¹ - 0.125 mA.cm ⁻² 155 mA.h.g ⁻¹ - 0.63 mA.cm ⁻²	[51]
Carbon sphere template method	100 – 500	Hollow Spheres	100 mA.h.g ⁻¹ - 10 C 150 mA.h.g ⁻¹ - 2 C - 200 cycle	[52]
Electro spinning method	230 – 270	Nan fibers	140-192 mA.h.g ⁻¹ - 0.5 C - first five cycles with a capacity loss of 1.0% percycle 87 - 170 mA.h.g ⁻¹ - first 30 cycles with a capacity loss of 1.6% per cycle at 1.5 C	[53]
Spray pyrolysis	980	Spherical	171-168 mA.h.g ⁻¹ – 50 cycle by heating at 800 °C Decreased from 172 to 129 mA.h.g ⁻¹ for 1000 °C heating LTO heated at 600, 800 °C have good retention capacity value on cycling while treating at 1000 °C has poor cycle properties	[54]
Composite molten salt method	500-3000	Octahedral	The LTO powder with molar ratio of LiCl/KCl = 1.5 achieves initial discharge capacity of 169 mA.h.g ⁻¹ charge/discharge efficiency of 94% at 0.2 C good rate performances from 0.2 to 5 C	[55]

1.13 Synthesis of LTO Using Sol-gel Method

Sol-gel process is widely used as a wet-chemical technique for the synthesis of inorganic materials. A colloidal solution (sol) acts as the pioneer for a mobilized network (or gel) of either separate particles or network polymers. Metal alkoxides are

the most widely used precursors, metal salts (such as chlorides and acetates), and organic metal compounds can undergo various forms of hydrolysis and poly condensation reactions. Sol-gel method has several advantages and it is more appropriate for commercialized application. The sol-gel technique makes no effect on environment and it can use as an aqueous solution. Size and morphology, homogeneity of the products, particle size, micro structure and mono disparity can easily control by this process [56]. Sol-gel process can also use for the application of understanding uniform distribution of ions in oxides, low fabrication cost, simple stoichiometric control and high rate of deposition, the temperature which is used in synthesis is low, heating time is shorter and crystal formation is better.

In getting LTO of higher electrochemical performance many efforts have been done through sol-gel method. Kim et al. [57] reported the synthesis of LTO by a novel sol-gel method with high energy ball milling (HEBM) of precursor. HEBM LTO exhibited the first capacity of 173 mA.h.g^{-1} and excellent cycle ability.

The starting materials used by Alias et al. [58] were lithium tert-butoxide and titanium isopropoxide, which were mixed together in ethanol and the residue was harvested and finally sintered at different temperatures ($700\text{-}1000 \text{ }^\circ\text{C}$) and times (1-5 h). Hao et al. [59] used triethanol amine (TEA) as the chelating agent, while Khomane and co-workers applied hexadecyl trimethyl ammonium bromide (CTAB) cationic surfactant for controlling the crystal growth of LTO. The typical synthetic procedure, CTAB was dissolved in 100 ml ethanol under continuous magnetic stirring. Four grams of lithium acetate dihydrate was also dissolved in above solution under magnetic stirring. Titanium (IV) isopropoxide was added drop wise to the above solution by keeping the mole ration $\text{Li: Ti} = 1: 1.25$. Temperature of the solution was raised to $90 \text{ }^\circ\text{C}$ and continuously stirred to form the gel. The gel was heated at $100 \text{ }^\circ\text{C}$ for 24 h in air and the precursor was decomposed at $400 \text{ }^\circ\text{C}$ for 4 h followed by calcinations at $800 \text{ }^\circ\text{C}$ for 12 h in air. The prepared LTO had average discharge capacity taken over 20 cycles is $\sim 60 \text{ mA.h.g}^{-1}$ a constant current density of 21.37 mA/g . They also reported that citric acid sol-gel method used to synthesize LTO, when a molar ratio R of citric acid to total metal ions is $1/2$, initial discharge capacity of LTO was exhibited 167 mA.h.g^{-1} at 23.5 mA.h.g^{-1} and a subsequent charge capacity of 151 mA.h.g^{-1} . Extensive research work is still going on this area for developing anode and/or cathode materials for high power lithium ion battery.

Individual doping of LTO with Zn^{2+} or Cu^{2+} were done by some research groups. So far our knowledge, co-doping of Zn^{2+} and Cu^{2+} into LTO using sol-get method haven't been done. Thus, in this thesis a series of Zn^{2+} and Cu^{2+} co-doped LTO material have been prepared for Li ion battery anode material.

1.14 Characterization techniques:

1.14.1 Fourier-Transform Infrared Spectroscopy (FTIR)

The attenuated total reflection (ATR) technique of FTIR is used to analyze the presence of functional groups of prepared LTO. Characterization was carried out using IRTracer-100 of Shimadzu corporation, Japan. Mainly P-O stretching vibration of PO_4^{3-} in the prepared LTO nanoparticles were identified by using ATR technique. No sample preparation is required for this analysis. One kind of crystals knob attached with the FTIR machine is used to identify the presence of functional groups of the prepared sample. The crystal knob has been kept clean and scratches free for each of the experiment. Firstly we placed a sample of LTO on the top of a flat surface. Then we mounted and adjusted the knob above the sample surface. Adjustment between knob and the sample surface was done in such as a way that a consistent contact is achieved between them. Afterwards, a black gripper was used to cover the sample surface. A computer based FTIR program was used to identify the functional groups of LTO. The entire FTIR spectrum of the prepared sample has been recorded in the range of 300 to 3800 cm^{-1} .



Figure 1.6: FTIR Machine

FTIR stands for Fourier Transform Infra-Red, the preferred method of infrared spectroscopy. In infrared spectroscopy, IR radiation is passed through a sample. Some of the infrared radiation is absorbed by the sample and some of it is passed through (transmitted). The resulting spectrum represents the molecular absorption and transmission, creating a molecular fingerprint of the sample. FTIR can provide information such as:

- (i) It can identify unknown materials
- (ii) It can identify the functional groups of a material.
- (iii) It can determine the amount of components in a mixture

An infrared spectrum represents a fingerprint of a sample with absorption peaks which correspond to the frequencies of vibrations between the bonds of the atoms making up the material. Because each different material is a unique combination of atoms, no two compounds produce the exact same infrared spectrum. Therefore, infrared spectroscopy can result in a positive identification (qualitative analysis) of every different kind of material. This method is used to characterize the prepared lithium titanate based materials. It has given useful information about Ti-O-Ti peak. The presence of other functional groups like hydroxyl and carboxyl has also been understood from their IR spectrum.

1.14.2 X-ray Diffraction (XRD)

X-ray diffraction studies on the prepared samples were carried out using a high resolution Bruker Advance D8 XRD (Figure 1.7) diffractometer in Bragg-Brentano geometry, with a $\text{CuK}\alpha 1$ monochromated beam ($\lambda = 0.15406 \text{ \AA}$) produced at 40 kV and 40 mA. Slight quantity of LTO has been loaded into sample holders by simply pouring it with. After that it was mounted on the diffractometer. The scanning range (2θ) was accomplished from $10\text{-}70^\circ$. This method was used to measure the phases existing in the prepared LTO.



Figure 1.7: XRD Machine

X-ray diffraction (XRD) is the supreme common method for characterizing crystal-like materials. This method relies on the double wave/particle nature of X-rays to find information about the structure of crystalline materials.

In crystalline materials dissimilar (Figure 1.8) sets of planes are designed by occasionally arranged electron shells of atoms. These planes are able to interact with the incident X-ray beam by forming constructive or destructive interferences. This is the process of diffraction. Different compounds have different diffraction patterns. A primary use of the technique is the identification and characterization of compounds based on their diffraction pattern.

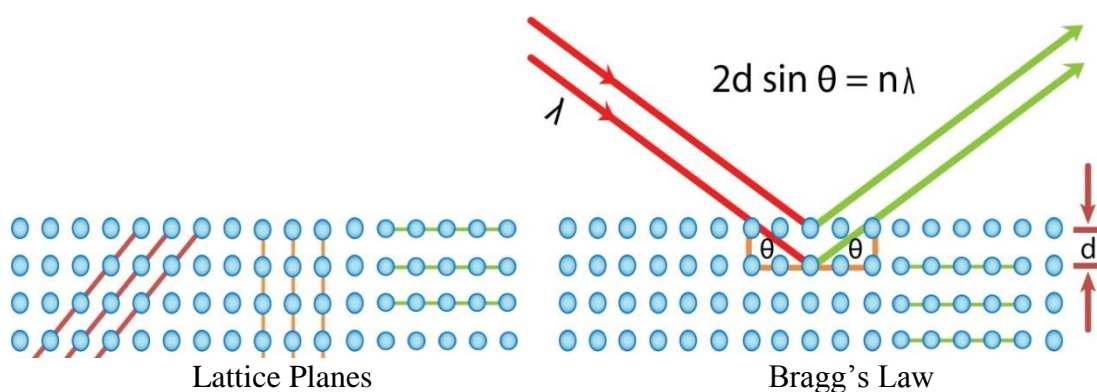


Figure 1.8: Schematics of Bragg's Law for the scattering of X-rays at periodic crystal lattice planes

The Bragg's Law is one of most important laws used for interpreting X-ray diffraction data. For a given set of lattice planes with an inter-plane distance of d , the condition

for constructive interference, resulting in a diffraction peak, can be simply written as (Equation 1.1)

$$n\lambda = 2d\sin\theta \text{ ----- (1.1)}$$

Where λ is the wavelength of the X-ray beam, θ represents the angle between incident X-ray beam and crystallographic planes and n an integer representing the order of the diffraction peak. With two parallel X-ray beams diffracted on parallel atomic planes a distance of d apart, the deeper beam travels an extra distance of $2d\sin\theta$, which is a multiple of the X-ray wavelength (λ) and an integer (n), if the two beams are in phase. Various d spacing of crystallographic planes can be obtained by scanning θ . When a beam of X-ray interacts finely with the atoms in sample, there must be a fraction of crystals with crystallographic planes orientated with a Bragg angle θ , at which Bragg diffraction can take place. With sample stage rotating with respect to the incident X-ray beam, a XRD pattern containing characteristic diffractions can be recorded by a detector. Such a XRD diffraction pattern is a fingerprint useful for identifying the crystal characteristic such as size, crystallinity, lattice parameters and phase with the help of a comprehensive XRD database. In this thesis study, XRD is used to identify crystal phases and volume of the unite cell.

1.14.3 Scanning Electron Microscopy (SEM)

A JEOL JSM-7600FJEOL was used in this study to get the surface morphology of the prepared LTO. A conductive carbon tape was fixed on the alumina plate. Then the 2-3 drops of the sample was placed on the conductive carbon tape. Later that the sample was permitted to dry for an adequate periods of time. Any extra powder on the sample plate was removed by an air blower. Lastly the sample plate was committed on the sample chamber for SEM operation.

At the first effort of action a vacuum pump was used to reach the level of vacuum essential to produce a reliable electron beam. A finely focused electron beam between 10 – 25 kV was irradiated on the sample under observation. A detector screens the scattered electron (SE) indicators and the brightness of the spot is measured by an improved version of the detected signal. The surfaces facing the light source look bright while those facing away range from grey to black.



Figure 1.9: Picture of a scanning electron microscope machine

The scanning electron microscope (SEM) is a powerful and frequently used instrument, in both academic and industry to study, for example, surface topography, composition, crystallography and properties on a local scale. SEM has an extremely large depth of focus and is therefore well suited for topographic imaging. Besides surface topographic studies the SEM can also be used for determining the chemical composition of a material, its fluorescent properties and the formation of magnetic domains and so on. The specimen is bombarded by a convergent electron beam, which is scanned across the surface. This electron beam generates a number of different types of signals, which are emitted from the area of the specimen where the electron beam is impinging (Figure 1.10).

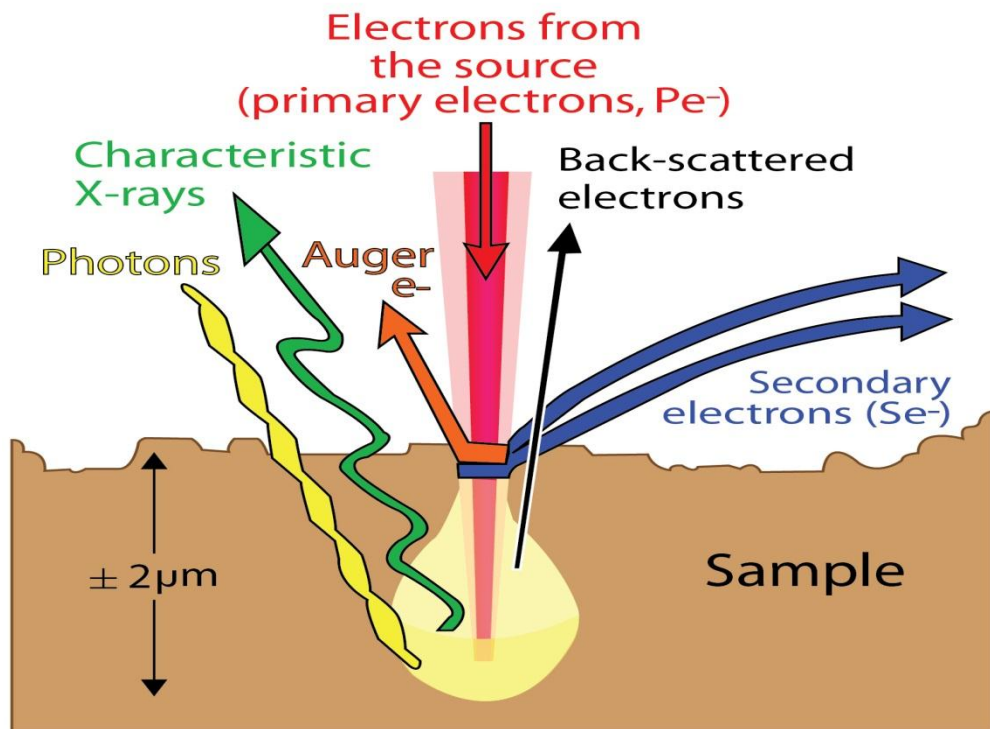


Figure 1.10: Working procedure of SEM

The induced signals are detected and the intensity of one of the signals (at a time) is amplified and used to as the intensity of a pixel on the image on the computer screen. The electron beam then moves to next position on the sample and the detected intensity gives the intensity in the second pixel and so on.

The working principle of the SEM is shown in Figure 1.11. For improved signal-to-noise ratio in the image, one can use a slower scan speed. This means that the electron beam stays a longer time at one position on the sample surface before moving to the next. This gives a higher detected signal and increased signal-to-noise ratio.

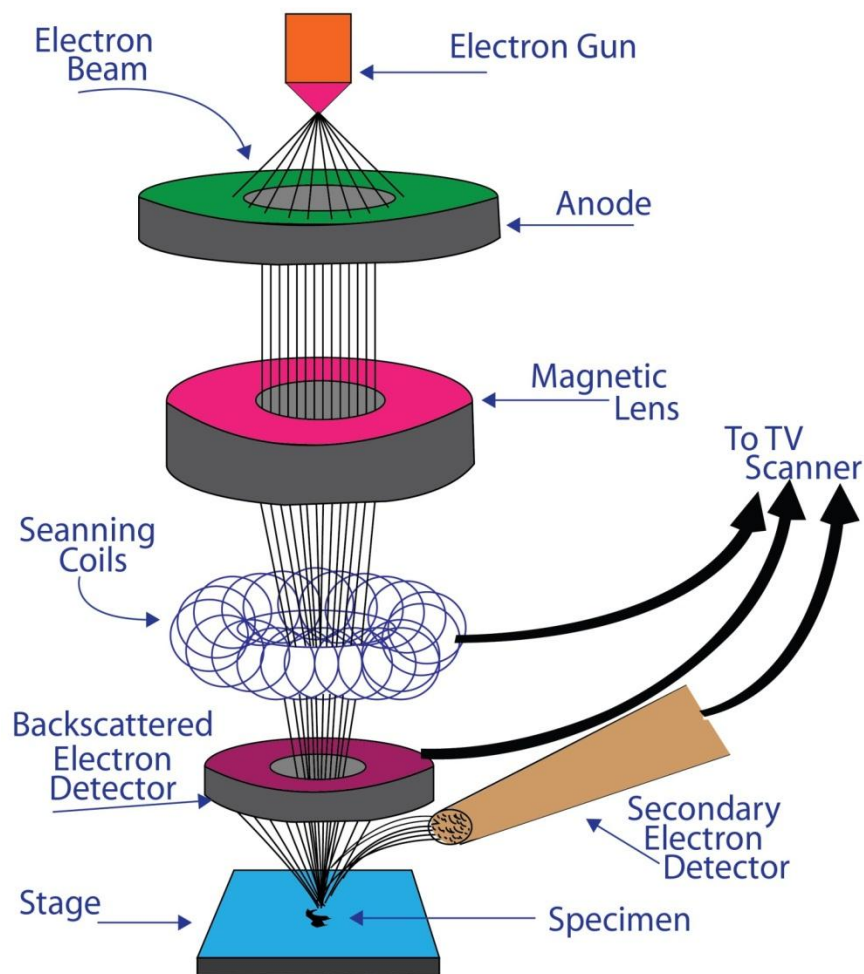


Figure 1.11: Schematic diagram of a SEM

1.15 Electrochemical Characterization Using Cyclic Voltammetry

Cyclic voltammetry is one of the most exploited techniques in electrochemical studies. Its primary advantage comes from the fact that it gives insight into both the half-reactions taking place at the working electrode, providing at the same time information about the chemical or physical phenomena coupled to the studied electrochemical reaction. Hence cyclic voltammetry is often considered as electrochemical spectroscopy. Although its usage is relatively minimal in quantitative food analysis, it is important to elaborate the principles of cyclic voltammetry, since every electro analytical study almost inevitably commences with this technique. In cyclic voltammetry, starting from an initial potential E_i , a staircase (Figure 1.12) potential sweep (or linear sweep in older potentiostat) is applied to the working electrode. After reaching a switching potential E_f , the sweep is reversed the potential

returns to its initial value. The main instrumental parameter in the cyclic voltammetry is the scan rate ($v^{1/2}dE=t$), since it controls the timescale of the voltammetric experiment. The useful scan rates range from 1 to 1000 mV/s, although scan rates of over 10 V/s are technically achievable. The instrumental output in cyclic voltammetric techniques is a current–potential curve, a cyclic voltammogram. The main features of the cyclic voltammogram are the cathodic and anodic peak potentials, the cathodic and anodic peak currents, and the formal (or half-peak) potential.

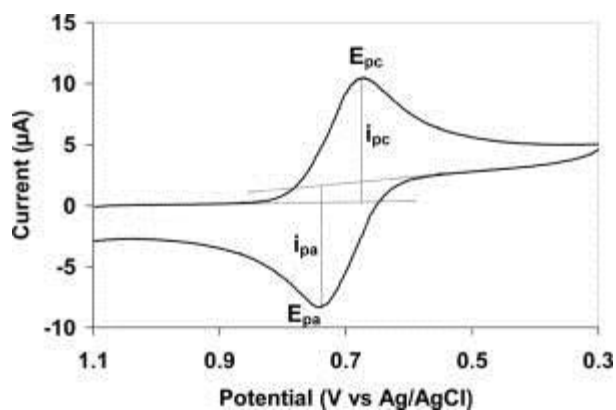


Figure 1.12: Cyclic Voltammogram response for a reversible redox couple

Chapter –II

Literature Review

2.1 Development History of Battery

The first electrochemical cell is discovered by an Italian physicist Alessandro Volta (1800) because he demonstrated that two different metals zinc and copper, could generate electric current by decomposing water and generating hydrogen when they were immersed in acidic electrolyte. This discovery was followed a few decades later by Michael Faraday's major advances in developing the laws of electrochemistry, and the subsequent development of rechargeable batteries with aqueous electrolytes, notably lead–acid (Gaston Plante 1859), nickel–cadmium (Waldemar Jungner, 1899), and nickel–iron (Thomas Edison, 1901) systems. Nickel–cadmium and nickel–iron batteries were therefore runners of modern-day nickel–metal hydride batteries, introduced into the market in 1989 [60].

Li-based rechargeable batteries were first proposed in the early 1960s and since then the battery has undergone several transformations. Initially, metallic Li was selected as the anode but it induced serious safety hazards because of dendritic Li grows and pierces the separator membrane during cycling and finally triggers short circuit [61]. The most inspiring breakthrough in LIB technology happened in 1991 owing to Sony Corporation's introduction of a high-voltage (~3.7 V) and high-energy $\text{Li}_x\text{C}_6/\text{non-aqueous liquid electrolyte/Li}_{1-x}\text{CoO}_2$ cell for portable electronic applications. Furthermore, the discovery of stable, liquid organic carbonate solvents allowed the reversible operation of these LIBs at high voltage, at least up to 4.2 V. And since 1991, graphite has remained the anode material of choice [60]. Table 2.1 lists the landmarks of the history of batteries.

Table 2.1: History of electrochemical cell development

Types of battery	Invented year	Battery inventor	Battery name
Primary battery	1800	Alessandro Volta	Voltaic pile
	1836	John Frederic Daniel	Daniel cell
	1844	William Robert Grove	Grove cell

	1860	Callaud	Gravity cell
	1866	Georges-Lionel Leclanché	Leclanchéwet cell
	1888	Carl Gassner	Zinc-carbon dry cell
	1955	Lewis Urry	Alkaline battery
	1970	No information	Zinc-air battery
	1975	Sanyo Electric Co.	Lithium-manganese cell
	2004	Panasonic Corporation	Oxyride battery
Secondary battery	1859	Raymond Gaston Planté	Plantélead-acid cell
	1881	Camille Alphonse Faure	Improved lead acid cell
	1899	Waldmar Jungner	Nickel- cadmium cell
	1901	Thomas Edison	Nickel-iron cell
	1946	Union Carbide Company	Alkaline manganese secondary cell
	1970	Exxon laboratory	Lithium-titanium disulfide
	1980	Moli Energy	Lithium-molybdenum disulfide
	1990	Samsung	Nickel-metal hydride
	1991	Sony	Lithium-ion
	1999	Sony	Lithium polymer

A LIB mainly consists of a cathode, an anode, electrolyte and a separator. The cathode materials are commonly Li-containing transition metal oxides with a layered structure (such as lithium cobalt oxide) or tunnel-structured materials (such as lithium manganese oxide). The anode materials include insertion-type materials (such as graphite, TiO_2 , etc.), conversion-type materials (such as iron oxides, nickel oxides, cobalt oxides, etc.), and alloying-type materials (such as Si, Sn, etc.). The electrolyte is supposed to be a good ionic conductor and electronic insulator. Most of the electrolytes are based on the solution of inorganic lithium salts dissolved in a mixture of two or more organic solvents. The function of the separator is to prevent short

circuit between the two electrodes and to provide abundant channels for transportation of Li ion during the process of charging/discharging.

2.2 Modification of LTO

Since the highest possible valence of Ti in LTO is (+4) for the oxidation state of Ti, electronic conductor of LTO is very poor and leads to low specific capacity and poor capabilities at high rate. Electrical conductivity of LTO has been attracted to increase for its great interests in the science and technology of lithium ion batteries. Many efforts have been done as described as follows:

- i) LTO is doping with noble metal or oxide nanoparticle. Such as, Ti^{4+} is replacing with some of M^{3+} or M^{4+} metals for preparing $Li_4Ti_5O_{12}$, for example $Li_{4/3-y/3}M_yTi_{5/3-2y/3}O_4$ (e.g., Fe^{3+} , Ni^{3+} , and Cr^{3+}), $Li_4M_yTi_{5-y}O_{12}$ (Al^{3+} , Mn^{4+} , V^{4+} , and Fe^{3+}), and $Li_4Al_xTi_{5-x}O_{12-y}F_y$, (Fe^{3+} , Ni^{3+} , Cr^{3+} or Mg^{2+} doped), substituting Li or Ti by other metal cations, such as V^{5+} , Mn^{4+} , Ga^{3+} , Co^{3+} , Ta^{5+} , Cu^{2+} .
- ii) High electronic conductivity of a second phase is incorporated. For example, employing Ag [62] carbon and Cu or CuO_x as the conducting second phase and loading SnO_2 on LTO [63];
- iii) By adding of conductive fillers [64] for example carbon black;
- iv) Coating the surface with conductive material e.g, carbon and silver, and TiN thin film [65];
- v) The particle size is reduced by novel synthesis methods and obtains desired structure, especially the nanoparticles [64] including combustion synthesis method with different agents, and rheological method and
- vi) Nitridation to form oxynitride species on its surface [66].

2.3 Atomic Doping of LTO

Mainly doping has been used in the research field for increasing the poor electronic conductivity of LTO. It can be realized by doping various metal cations (V^{5+} , Mn^{4+} , Fe^{3+} , Al^{3+} , Ga^{3+} , Co^{3+} , Cr^{3+} , Ni^{2+} , Mg^{2+}) into Li or Ti sites, or other anions such as Br^- , F^- into O sites. Theoretically doping of cation on LTO effects on the electronic conductivity and it has been reported. According to the first-principles of local density calculations, the electronic conduction of LTO improves by Cr or Mg doping, while

Ni or Fe does not have such effect. Wen et al. [66] experimented that Ag, Cu, C and the Cu_xO oxide composite-based LTO material increase its electronic conductivity significantly. Also co-doping, such as Mg-Al, Al-F, Mg-V, can also enhance its electronic conductivity.

2.4 Transition Metal Doping

Doping of transition metal increase the interest to improve electrical conductivity of electrode including cathode materials such as LiCoO_2 , LiNiO_2 , LiMnO_2 and anode materials. If the conductivity of LTO is low then it leads to a low specific capacity and the application in industrial market is limiting. LTO doping with transition metal is distinctly a better way to solve this problem. Fourth period of transition metal has been studied. The properties of transition metal doping on the LTO is summarized in Table 2.2.

Table 2.2 The properties of LTO doped by transitional metal

Doped formula	Function	Electrochemical performance	Advantages	Ref.
Transition metal in the fourth period				
V^{5+} $\text{Li}_4\text{Ti}_{5-x}\text{V}_x\text{O}_{12}$ ($0 \leq x \leq 0.3$)	Lattice parameter has no effect, blue shift on Raman bands of Li-O and Ti-O vibration. When V increases then discharge capacity decreases	$\text{Li}_4\text{Ti}_{4.9}\text{V}_{0.1}\text{O}_1$ 183 mA.h.g^{-1} -100 cycles -0.5-2.0 V 229 mA.h.g^{-1} - 130 cycle	Better-quality reversible capacity Respectable cycling performance Small cost	[67]
$\text{Li}_4\text{Ti}_{2.5}\text{Cr}_{2.5}\text{O}_{12}$	When average particle size increases, conduction is little higher, crystallite size has no effect	151 mA.h.g^{-1} - 2 C 146 mA.h.g^{-1} - 5 C	Cycle ability rate is high (up to 5 C)	[68]
Mn^{n+} (n=2,3,4) $\text{Li}_{1.333-x/3}\text{Mn}_x\text{Ti}_{1.667-2x/3}\text{O}_4$, $\text{Li}_{1.333-x/6}\text{Mn}_x$	Spinel structure has no changed, conductivity and lattice parameter are decreased with the	-----	-----	[69]

$Ti_{1.667-x}O_4$ ($x=0.05, 0.167, 0.25, 0.50$)	Mn content increasing			
Fe^{3+} $Li_4Ti_{4.75}Fe_{0.25}O_2$	Capacity is decreased.	106 mA.h.g ⁻¹	-----	[70]
Co^{3+} $Li_{3.85}Co_{0.15}Ti_{4.9}O_{1.9}$	Electric conductivity and lattice parameters are decreased and also electrochemical performance are decreased	171.9 mA.h.g ⁻¹ - 0.15 mA.cm ⁻² 155.2 mA.h.g ⁻¹ - 40 cycle	-----	[71]
Cu LTO/Cu composite	Electronic conductivity is improved, almost 2 orders of magnitude higher than the pristine $Li_4Ti_5O_{12}$	209.2 mA.h.g ⁻¹ - 1C-1st cycle 142.5 mA.h.g ⁻¹ - 10 C - 1st cycle	Discharge capacity rate is high Cycling stability	[72]
Cu^{2+} $Li_4Ti_5Cu_xO_{12+x}$	Lattice parameter progressively increases with x, optimal composition is $Li_4Ti_5Cu_{0.15}O_{12.15}$	163.3 mA.h.g ⁻¹ - 1st cycle- $x = 0.075$ 169.5 mA.h.g ⁻¹ - 1st cycle $x = 0.15$ 177.0 mA.h.g ⁻¹ - 1st cycle- $x = 0.3$ 187.2 mA.h.g ⁻¹ - 1st cycle- $x=0.6$ Little capacity loss after 50 cycles.	Rate performance is high	[73]
Transition metal in other period				
Ag LTO/Ag composite	It does not enter into the spinel structure, electrochemical performance improves.	114.4 mA.h.g ⁻¹ - 25 cycles- 10 C	Reversible capacity is improved Cycling stability is good	[74]

Zr $\text{Li}_4\text{Ti}_{5-x}\text{Zr}_x\text{O}_{12}$ ($x=0, 0.05, 0.1, 0.2$)	Structural characteristics does not change, particle size and morphology greatly affected, optimum composite is $\text{Li}_4\text{Ti}_{4.9}\text{Zr}_{0.1}\text{O}_{12}$	Increasing the rate capacity less degraded. 141 mA.h.g ⁻¹ -3 C - $x = 0.05$ 146 mA.h.g ⁻¹ -3 C- $x = 0.1$ 126 mA.h.g ⁻¹ -3 C- $x = 0.2$	Improve the rate capability.	[75]
Nb $\text{Li}_4\text{Ti}_{4.95}\text{Nb}_{0.05}\text{O}_{12}$	Electronic conductivity and Li-ion diffusivity are also improved	169.1 mA.h.g ⁻¹ -1 C 115.7 mA.h.g ⁻¹ - 10 C- 100 cycles	Rate capability is excellent	[76]

Ti^{4+} and Li^+ partially substituted in the spinel with V^{5+} as $\text{Li}_4\text{Ti}_{5-x}\text{V}_x\text{O}_{12}$ was proposed by Yi et al. [67]. The specific capacities of discharge $\text{Li}_4\text{Ti}_{5-x}\text{V}_x\text{O}_{12}$ are 167, 171, 167, and 166 mA.h.g⁻¹ cycling in the voltage range of 1.0-2.0 V, when $x = 0, 0.1, 0.15$, respectively; 208, 240, and 234 mA.h.g⁻¹ cycling in 0.5-2.0 V, when $x = 0, 0.1, 0.15$, respectively; 303, 348, 333, 323, 312, and 254 mA.h.g⁻¹ cycling in 0.0-2.0 V, when $x = 0, 0.1, 0.15, 0.2, 0.25, 0.3$, respectively. Its capacity is higher than pure LTO spinel. All the results specifying that $\text{Li}_4\text{Ti}_{4.9}\text{V}_{0.1}\text{O}_{12}$ initial discharge capacity has highest and cycling performance in the range of 0.0-2.0 V or 0.5-2.0 V. They further reported $\text{Li}_4\text{Ti}_{4.95}\text{V}_{0.05}\text{O}_{12}$ also delivering discharge capacity of 218.4 mAh/g after 50 cycles. Lower electrode polarization and higher lithium ion diffusivity in solid-state body of $\text{Li}_4\text{Ti}_{4.95}\text{V}_{0.05}\text{O}_{12}$ implies that vanadium doping is beneficial to the reversible intercalation and de-intercalation of lithium ions.

Capsoni et al. was demonstrated Mn-substituted LTO [77]. By increasing of Mn content the Fd3m spinel structure of the lithium titanate is preserved and decreases the lattice parameter. The tetrahedral site is occupying by Mn^{2+} ions exclusively up to 10% with Mn-substituted LTO. Both on octahedral and tetrahedral sites distribute by Mn^{3+} ions, with a constant value on the tetrahedral one, independent of the total Mn amount; Mn^{4+} ions are not detected. The presence of Mn ions on the tetrahedral site,

which extrudes Li content in the material and decreases the electronic conductivity of spinel LTO.

Various amount of Co can influence the crystallize structure of spinel. Jovic et al. [78] reported that in the composition of $\text{Li}_{1.33x}\text{Co}_{2-2x}\text{Ti}_{1+0.67x}\text{O}_4$ ($0 \leq x \leq 1$), space group is Fd3m at $0 \leq x \leq 0.40$ or $x = 1$, the space group is P4₃2 at $0.50 \leq x \leq 0.875$. The electrochemical performance of spinel LTO has been demonstrated to improve by copper doping. Wang et al. [79] reported the Cu^{2+} doping into LTO as $\text{Li}_4\text{Ti}_5\text{Cu}_x\text{O}_{12+x}$, which largely improves rate performance compared with LTO. The optimal nominal composition is $\text{Li}_4\text{Ti}_5\text{Cu}_{0.15}\text{O}_{12.15}$ with increasing the conductivity of LTO by many orders of magnitude. When $x = 0, 0.075, 0.15, 0.30, \text{ and } 0.6$, the conductivity of $\text{Li}_4\text{Ti}_5\text{Cu}_x\text{O}_{12+x}$ is $4.2 \times 10^{-7}, 3.0 \times 10^{-6}, 4.7 \times 10^{-6}, 5.3 \times 10^{-6}$ and $8.2 \times 10^{-6} \text{ S}\cdot\text{cm}^{-1}$, respectively, while the conductivity of $\text{Li}_4\text{Ti}_5\text{O}_{12}$ at room temperature is less than $10^{-13} \text{ S}\cdot\text{cm}^{-1}$. Huang et al. [80] also reported that the Cu additive effectively improves the electronic conductivity and electrochemical performance of the pristine LTO, especially at high rate (Table 2.3).

Table 2.3: Comparison of discharge capacity and cycling stability of the LTO and doped Cu- LTO anode materials [80]

Rate ^a (C)	Anode materials	Capacity of discharge cycle (mA.h.g ⁻¹)	
		1 st	10 th
1	Doped Cu- LTO	209.2	171
	LTO	180.6	164.2
2	Doped Cu- LTO	184.8	166.6
	LTO	162.2	155
4	Doped Cu- LTO	173.4	153.6
	LTO	150.7	117.3
8	Doped Cu- LTO	165.7	144.6
	LTO	98.9	72.5
10	Doped Cu- LTO	142.5	141.6
	LTO	80.3	61.2

a: charge-discharge rate

2.5 Doped by Metal in the Main Group

Some metals in the main group doping have attracted considerable interest and studied on the electric conductivity improvement of spinel lithium titanate. The metals studied presently are in the second, third and fourth period, their function and properties are summarized in Table 2.4.

Table 2.4: Doping properties of LTO by metal in the main group

Metals	Formation	Properties and electrochemical performance	Ref
Li	$\text{Li}_{4+x}\text{Ti}_{5-x}\text{O}_{12}$	Appropriate amount of Li ($x = 0.1$) doping electronic conductivity and conductivity of lithium-ion are improves, in a result rate performance is better compared with the undoped $\text{Li}_4\text{Ti}_5\text{O}_{12}$	[81]
Mg	$\text{Li}_{4-x}\text{Mg}_x\text{Ti}_5\text{O}_{12}$	LTO conductivity is increased by $\text{Li}_{4-x}\text{Mg}_x\text{Ti}_5\text{O}_{12}$ of different orders of magnitude When $x=1.0$, then $\text{Li}_3\text{MgTi}_5\text{O}_{12}$ conductivity is increased to $10^{-2} \text{ S cm}^{-1}$ from $10^{-13} \text{ S cm}^{-1}$ for pristine $\text{Li}_4\text{Ti}_5\text{O}_{12}$ The rate properties of $\text{Li}_4\text{Ti}_5\text{O}_{12}$ are improved. 3 % of Mg-doped LTO shows the excellent charge (145 mA.h.g^{-1}) and discharge capabilities (149 mA.h.g^{-1}) with the current density of 0.1 C	[82]
Al	$\text{Li}_{4-x}\text{Al}_x\text{Ti}_5\text{O}_{12}$	Electronic conductivity is enhanced with lithium ionic conductivity decreases. Stability of cycling at high charge & discharge rate is significantly increased $\text{Li}_{3.9}\text{Al}_{0.1}\text{Ti}_5\text{O}_{12}$ is an optimal composition, it shows the rate performance best under this investigational condition	[83]

Ga	$\text{Li}_{3.82}\text{Ga}_{0.15}\text{Ti}_{4.9}\text{O}_{11.94}$	LTO capacity is increased by Ga^{3+} to various extent with the persistent current density of $0.15 \text{ mA}\cdot\text{cm}^{-2}$ among the cut off voltages of 2.3 and 0.5 V, the 1 st discharge capacity of LTO is $199.8 \text{ mA}\cdot\text{h}\cdot\text{g}^{-1}$ At the density of current $0.15 \text{ mA}\cdot\text{cm}^{-2}$ among 0.5 and 2.3 V, the changeable capacities subsequently 40 cycles is $165.5 \text{ mA}\cdot\text{h}\cdot\text{g}^{-1}$ with the loss of capacity 4.39%	[84]
----	---	---	------

Li and Mg have been demonstrated to improve the electrochemical performance due to the increasing of conductivity. Mg has been proved to be a good substitutional element in the spinel lithium titanate, doping Mg enhances greatly the conductivity of lithium titanate. Since these two metals obey the diagonal relationship, it is understandable that they have similar function while doping. Al has been investigated to have an optimal composition as $\text{Li}_{3.9}\text{Al}_{0.1}\text{Ti}_5\text{O}_{12}$, which shows the best rate performance. Be, which has the similar properties according to the diagonal relationship, may also obtain an optimal composition resulting in the best electrochemical performance by doping into LTO. However, further investigations are needed to confirm the prediction.

2.6 Doped by Non-metal in Carbon Group

Carbon is usually employed to modify electrode materials (e.g. LTO) to improve the electrochemical performance due to its low cost and good conductive property. There are mainly three categories of carbon modification on LTO anode material; namely, carbon coating on the surface, carbon doped into the nanostructure, and carbon existed as a secondary phase by forming a composite. Carbon modified LTO can improve the electrochemical performance in terms of rate capability, lithium storage capacity and capacity retention. The reasons for such enhancement in the performance are:

The carbon acts as bridges for electron pathways that electrically interconnect the LTO particles hence effectively improves the electronic conductivity of the hybrid

material. The different morphology (e.g. nanoparticles, nanotube) or category (e.g. graphene, amorphous carbon) of carbon would improve the electric conductivity. The nano sized LTO particles in the hybrid material provide a large electrode/electrolyte contact surface, shorten lithium diffusion path and allow fast electron/ion diffusion. The combined two parts is expected to provide LTO electrode with fast kinetics and lead to enhanced electrochemical performance compared with the bulk LTO.

Lin et al. [85] reported LTO/C composite improves reversible capacity and rate capabilities. The pyrolytic carbon incorporated into the spinel LTO particle reduces grain size and improve electronic conductivity, which is contributed to the electrochemical performances of LTO. The initial specific capacity of the composite is $130.0 \text{ mA}\cdot\text{h}\cdot\text{g}^{-1}$ at $8.60 \text{ mA}\cdot\text{cm}^{-2}$ and excellent cycle performance is still maintained with the current density increase. Liu et al. [86] reported LTO/C composite synthesized at $800 \text{ }^\circ\text{C}$ for 15 h under argon, containing 0.98 wt% of carbon. The composite exhibits better electrochemical properties compared with the pristine LTO due to the enhanced electrical conductive network of the carbon coating on the particle surface. The composite can deliver a capacity of $173.9 \text{ mA}\cdot\text{h}\cdot\text{g}^{-1}$ at 0.1 C rate while that of pure LTO is only $165.8 \text{ mA}\cdot\text{h}\cdot\text{g}^{-1}$. Huang et al. [87] reported that LTO/carbon nano-tubes present an excellent rate capability and capacity retention. Its discharge capacities are 145 and $135 \text{ mA}\cdot\text{h}\cdot\text{g}^{-1}$, at the rate of 5 C and 10 C, respectively. After 500 cycles at 5 C, the discharge capacity retains as $142 \text{ mA}\cdot\text{h}\cdot\text{g}^{-1}$ recently, Li et al. [88] further reported the composite of LTO/carbon nanotubes exhibiting better electrochemical performance than a LTO carbon composite. In addition, they investigated LTO graphitized carbon nanotubes composite, which shows high specific capacity and good rate capability. The initial discharge capacity of the composite is $163 \text{ mA}\cdot\text{h}\cdot\text{g}^{-1}$ at 0.5 C. Even at 10.0 C, its initial discharge capacity can reach $143 \text{ mA}\cdot\text{h}\cdot\text{g}^{-1}$, and $132 \text{ mA}\cdot\text{h}\cdot\text{g}^{-1}$ after 100 cycles, which is about 86% of its capacity after the same number of cycles at 1.0 C ($154 \text{ mA}\cdot\text{h}\cdot\text{g}^{-1}$).

Applying Sn as anode, high capacity of $990 \text{ mA}\cdot\text{h}\cdot\text{g}^{-1}$ can be achieved, however, Sn anode is unstable and can expands the volume as high as 360% than its original volume during Li insertion and extraction. One method to utilize the high capacity of Sn is to use it as a doping element. Cai et al. [89] reported that LTO/Sn composite displays much higher discharge capacity than pure LTO. LTO/Sn composite displays the first discharge capacity of $442 \text{ mA}\cdot\text{h}\cdot\text{g}^{-1}$ at current density of $100 \text{ mA}\cdot\text{h}\cdot\text{g}^{-1}$ and a

capacity of 224 mA.h.g^{-1} , which is higher than 195 mA.h.g^{-1} for the pure LTO, after 50 cycles at 100 mA/g current density. Si has a capacity of 1000 mA.h.g^{-1} , which is much higher than that of LTO. Its high capacity may be attributed to improve the capacity of LTO if it is doped into the spinel. Further work on the Si doping is certainly worth performing.

2.7 Purpose of the Research Work

From the above discussion it is obvious that there is no doubt that great markets exist for higher energy density batteries and increasing research efforts to develop high-power and high-capacity LIBs. Current commercial LIBs are limited by the capacity of their electrode materials. Although doping different metals possesses the highest specific capacity as anode material for LIBs. LTO is one of the competent electrode material and demands still further development on charge capacity issue. Considering the all above facts the specific objectives of this thesis are given below:

- i) LTO will be doped using proper amount of Zn^{2+} and Cu^{2+} . A series of novel metal doped LTO material have prepared by adjusting the cation concentration.
- ii) Particle size, surface morphology and crystal structure of the prepared LTO based anode materials have examined using SEM and XRD.
- iii) An electrochemical work related to lithium ion battery for the prepared LTO oxides has explored.

Chapter – III

Experimental Technique

This chapter describes the experimental setup and characterization technique of my research work. LTO nanoparticle was prepared by sol-gel method. The prepared materials were then characterized using FTIR, XRD and SEM. Electrode was prepared using the synthesized material. The battery was then assembled and characterized using cyclic voltammetry technique. Details about the source of different chemicals, instrumentations and procedure of the methods are given in the following sections.

3.1 Chemicals

All chemicals and solvents used in the synthetic and analytical work were analytical grade obtained from different international chemical company (E. Merck Germany, Loba Chemie and Gelon, P.R. China). The used chemicals were cited below.

Table 3.1: List of all chemicals

SL No	Compounds name	Company
i)	Lithium hydroxide monohydrate (LiOH.H ₂ O)	Merck, Germany
ii)	Titanium isopropoxide (C ₁₂ H ₂₄ O ₄ Ti)	Merck, Germany
iii)	Zinc nitrate hexa hydrate (Zn(NO ₃) ₂ .6H ₂ O)	Loba Chemie, India
iv)	Copper nitrate tri hydrate (Cu(NO ₃) ₂ .3H ₂ O)	Merck, Germany
v)	Citric acid (C ₆ H ₈ O ₇)	Loba Chemie, India
vi)	Ethylene diaminetetraacetic acid (C ₁₀ H ₁₆ N ₂ O ₈)	Merck, Germany
vii)	Ammonia solution (NH ₄ OH)	Merck, Germany
viii)	Acetylene black	Gelon, P.R. China
ix)	Polypropylene films	Gelon, P.R. China
x)	Polyvinylidene fluoride (PVDF)	Gelon, P.R. China
xi)	N- Methyl-2- pyrrolidone (C ₅ H ₉ NO)	Gelon, P.R. China
xii)	Lithium hexafluoro phosphate (LiPF ₆)	Gelon, P.R. China
xiii)	Ethylene carbonate (C ₃ H ₄ O ₃)	Gelon, P.R. China

xiv)	Ethyl methyl carbonate (C ₄ H ₈ O ₃)	Gelon, P.R. China
xv)	Dimethyl carbonate (C ₃ H ₆ O ₃)	Gelon, P.R. China
xvi)	Copper foil	Gelon, P.R. China
xvii)	Lithium wire	Gelon, P.R. China

3.2 Characterization Equipment

Synthesis and chemical analysis and some characterization have been done in the Department of Chemistry, KUET, Khulna. In addition some other characterization of the synthesized materials has been performed in Bangladesh Council of Scientific and Industrial Research (BCSIR), Dhaka, Bangladesh. Numerous equipment's were used during the research work and the list of them was given following table.

Table 3.2: Information of the instruments used in this experiment

Instrument name	Origin
pH Meter	BT 675, BOECO, Germany
Oven	Gemmy Industrial Corporation
FTIR Spectrometer	IRTracer-100, Shimadzu Corporation, Japan
Analytical Balance	ATY 224, Shimadzu Corporation, Japan
X-ray Diffraction	Bruker Advance D8 XRD, Germany
Scanning Electron Microscopy	JEOL JSM-7600FJEOL, USA

3.3 Preparation Method for LTO Based Anode Material

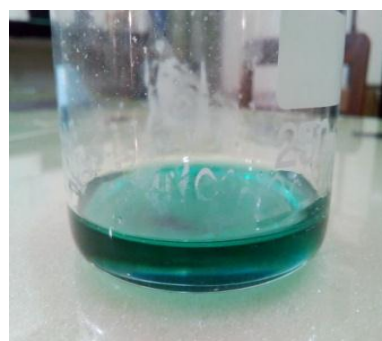
Zn²⁺ and Cu²⁺ doped LTO anode materials were prepared by a modified sol-gel method using EDTA-CA as co-chelating agents. A stoichiometric amount of lithium hydroxide monohydrate (LiOH.H₂O), titanium isopropoxide (C₁₂H₂₈O₄Ti), copper nitrate trihydrate Cu(NO₃)₂.3H₂O and zinc nitrate hexahydrate Zn(NO₃)₂.6H₂O were used as raw materials and dissolved into water. In the meantime, the EDTA and CA were pre-dissolved in ammonia, while the molar ratio of total metal ions to EDTA and to CA was kept at 1:1:2. Ammonia was added to keep pH value of the solution constant at about 7.0. Then the above solutions were mixed thoroughly, stirred. Finally it was heated at 80 °C till the redundant evaporated. The resulting transparent gel was heat-treated in an electric oven at 240 °C over 6 h to yield metal doped LTO precursor. Then the solidified precursor was calcined under open air at 750 °C for 5 h

to obtain metal doped LTO powders. The aforementioned method was used to prepare the following novel metal doped LTO based anode materials.

- 1) $\text{Li}_4\text{Ti}_5\text{O}_{12}$
- 2) $\text{Li}_4\text{Ti}_{4.5}\text{Cu}_{0.25}\text{Zn}_{0.25}\text{O}_{12}$
- 3) $\text{Li}_4\text{Ti}_{4.6}\text{Cu}_{0.20}\text{Zn}_{0.20}\text{O}_{12}$
- 4) $\text{Li}_4\text{Ti}_{4.70}\text{Cu}_{0.15}\text{Zn}_{0.15}\text{O}_{12}$
- 5) $\text{Li}_4\text{Ti}_{4.8}\text{Cu}_{0.10}\text{Zn}_{0.10}\text{O}_{12}$
- 6) $\text{Li}_4\text{Ti}_{4.9}\text{Cu}_{0.05}\text{Zn}_{0.05}\text{O}_{12}$
- 7) $\text{Li}_{3.9}\text{Ti}_5\text{Cu}_{0.05}\text{Zn}_{0.05}\text{O}_{12}$
- 8) $\text{Li}_{3.9}\text{Ti}_{4.9}\text{Cu}_{0.10}\text{Zn}_{0.10}\text{O}_{12}$
- 9) $\text{Li}_{3.8}\text{Ti}_5\text{Cu}_{0.10}\text{Zn}_{0.10}\text{O}_{12}$



(i) Heating and stirring of raw materials



(ii) Gel is formed after the reaction



(iii) Dried at 240 °C in an electric oven



iv) Take out from beaker



(v) After grinding



(vi) After calcinations at 750 °C



(vii) Storage of the desired LTO composite in a vial

Figure 3.1: Pictorial view of the synthesized LTO based composite materials

3.4 Fabrication of Electrode

To fabricate the anodes for the battery test cells, the working electrode was prepared as follows. Active materials (80%) were mixed with acetylene black (10%) as conducting agent, and polyvinylidene fluoride (PVDF) (10%) as binder in N-methylpyrrolidone (NMP). The blended slurries were pasted onto an aluminum foil, and the electrode was dried at 100 °C for 5 h in an oven. The electrolyte used was 1M LiPF₆ solvent in a 1:1:1 (vol%) mixture of ethylene carbonate (EC), ethylmethyl carbonate (EMC), and dimethyl carbonate (DMC). Test cells were assembled using Li foil as cathode and polypropylene (PP) film as the separator.

Chapter – IV

Results and Discussion

To sub side the energy catastrophe of fossil fuels and to reduce the global warming effect from huge production of carbon dioxide, it is important to advance the next generation electric vehicles or hybrid electric vehicles with high powder and energy density are required for energy storage devices [90]. LTO based anode materials especially the spinel lithium titanate is such a likely candidate for the anode electrode material in high power and energy Li-ion batteries. The importance of this thesis is the preparation of co-doped LTO anode materials having high power by sol-gel method for Li ion battery. Different ratio Cu and Zn are co-doped into LTO for the preparation of anode materials. One pure and three Cu and Zn are co-doped LTO based anode materials of varying ratio of metals have been prepared. The prepared LTO materials were then characterized by using FTIR, XRD and SEM. The results of this study has been presented and discussed in this chapter.

4.1 FTIR Spectra Analyses of Prepared LTO Based Materials

The FTIR spectra of the prepared pure LTO ($\text{Li}_4\text{Ti}_5\text{O}_{12}$), $\text{Li}_4\text{Ti}_{4.9}\text{Cu}_{0.05}\text{Zn}_{0.05}\text{O}_{12}$, $\text{Li}_{3.9}\text{Ti}_5\text{Cu}_{0.05}\text{Zn}_{0.05}\text{O}_{12}$ and $\text{Li}_{3.9}\text{Ti}_{4.9}\text{Cu}_{0.1}\text{Zn}_{0.1}\text{O}_{12}$ are presented in Figure 4.1-4.4, respectively. The presence of possible functional groups and phase purity of the materials can be confirmed by FTIR spectra which is scanned with in the wave number range 400 to 4000 cm^{-1} . During preparation Li^+ source reacts with $\text{C}_{12}\text{H}_{28}\text{O}_4\text{Ti}$ while lithium ion migrated into the nano-structure of $\text{C}_{12}\text{H}_{28}\text{O}_4\text{Ti}$ to form LTO ($\text{Li}_4\text{Ti}_5\text{O}_{12}$). As this reaction ended with mixed oxide formation so it was carried out relatively at higher temperature, 750 °C. So during the sintering process C-H bonds might be broken and there will be no peak in IR spectra for C-H stretching and bending. It is seen the following figures that there is no peak at around 2800 - 3100 cm^{-1} for the C-H stretching and the same at around 1000-1200 cm^{-1} for C-H bending. Instead of broad peaks few sharp but small peaks are present more than 3500 cm^{-1} may be attributed to the stretching vibrations of hydroxyl (O-H) originating from Ti-O-H [91]. In the finger print region sharp low frequency band observed at 669.30, 650.01, 617.22, 597.93, 572.86 cm^{-1} may be denoted the symmetric stretching

vibrations of Ti-O-Ti bonds of TiO_6 octahedron. Similar statements can be accomplished for $\text{Li}_4\text{Ti}_{4.9}\text{Cu}_{0.05}\text{Zn}_{0.05}\text{O}_{12}$ (finger print region sharp low frequency band observed at 719.45, 669.30, 650.01, 617.22, 607.58 cm^{-1}), $\text{Li}_{3.9}\text{Ti}_5\text{Cu}_{0.05}\text{Zn}_{0.05}\text{O}_{12}$ (finger print region sharp low frequency band observed at 719.45, 650.01, 617.22, 570.93 cm^{-1}) and $\text{Li}_{3.9}\text{Ti}_{4.9}\text{Cu}_{0.1}\text{Zn}_{0.1}\text{O}_{12}$ (finger print region sharp low frequency band observed at 719.45, 669.30, 650.01, 617.22, 609.51 cm^{-1}) because of low frequency bands found below 800 cm^{-1} [92, 93]. Strong stretching bands at 2360.87, 2341.58 and 2331.94 cm^{-1} can be assigned to the Ti-O bonds in the prepared pure LTO material and corresponds to the published results. Similar stretching bands for Ti-O bonds can be assigned in case of $\text{Li}_4\text{Ti}_{4.9}\text{Cu}_{0.05}\text{Zn}_{0.05}\text{O}_{12}$ (at 2358.94, 2341.58 and 2331.94 cm^{-1}), $\text{Li}_{3.9}\text{Ti}_5\text{Cu}_{0.05}\text{Zn}_{0.05}\text{O}_{12}$ (at 2358.94, 2341.58 and 2331.94 cm^{-1}) and $\text{Li}_{3.9}\text{Ti}_{4.9}\text{Cu}_{0.1}\text{Zn}_{0.1}\text{O}_{12}$ (at 2360.87, 2341.58 and 2331.94 cm^{-1}), respectively [92]. The stretching bands for Ti-O-Ti and Ti-O bonds are also summarized in the Table 4.1.

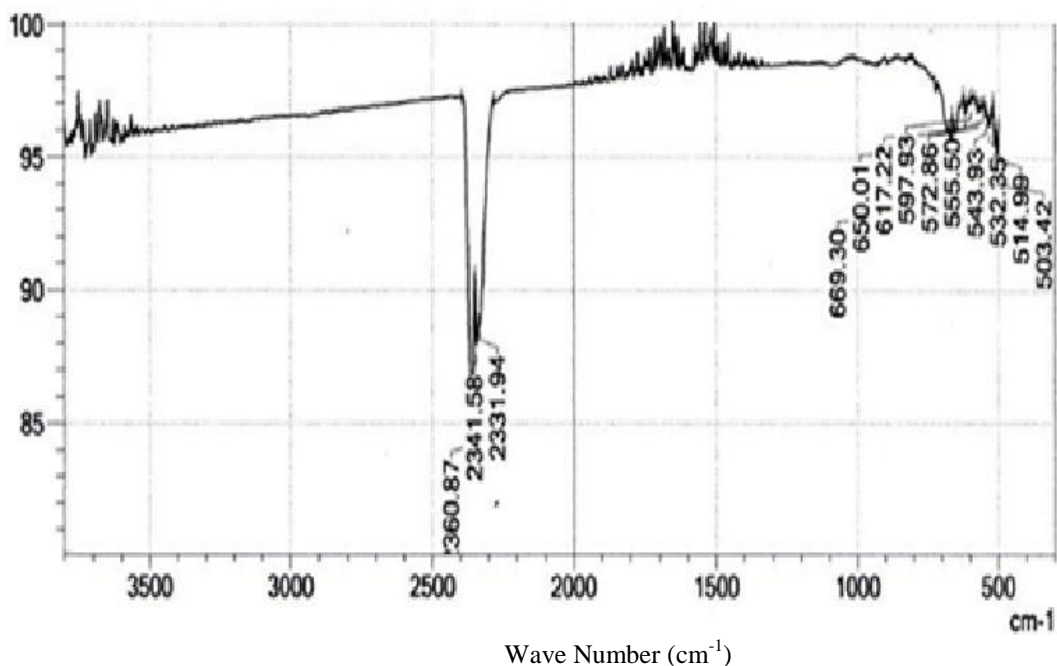
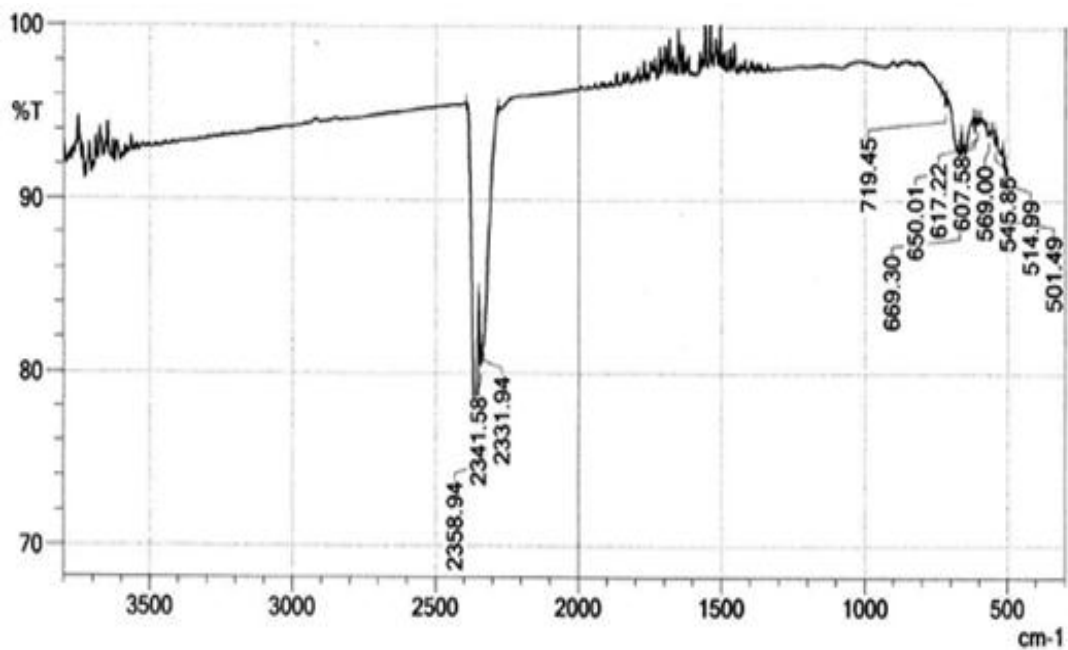
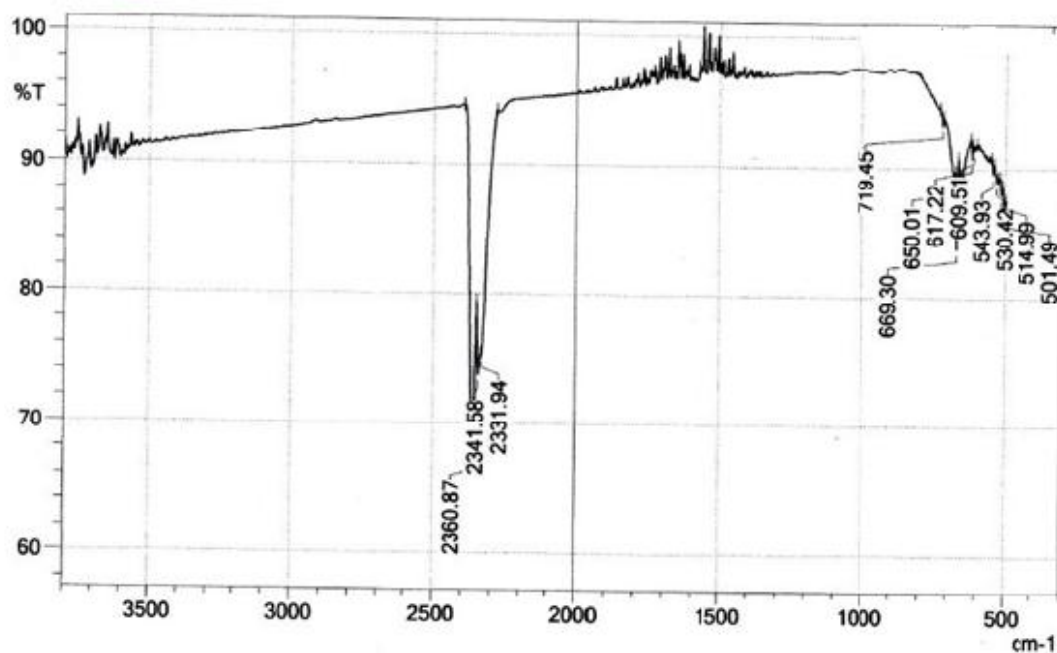


Figure 4.1: FTIR spectrum of pure LTO ($\text{Li}_4\text{Ti}_5\text{O}_{12}$)



Wave Number (cm^{-1})

Figure 4.2: FTIR spectrum of $\text{Li}_4\text{Ti}_{4.9}\text{Cu}_{0.05}\text{Zn}_{0.05}\text{O}_{12}$



Wave Number (cm^{-1})

Figure 4.3: FTIR spectrum of $\text{Li}_{3.9}\text{Ti}_5\text{Cu}_{0.05}\text{Zn}_{0.05}\text{O}_{12}$

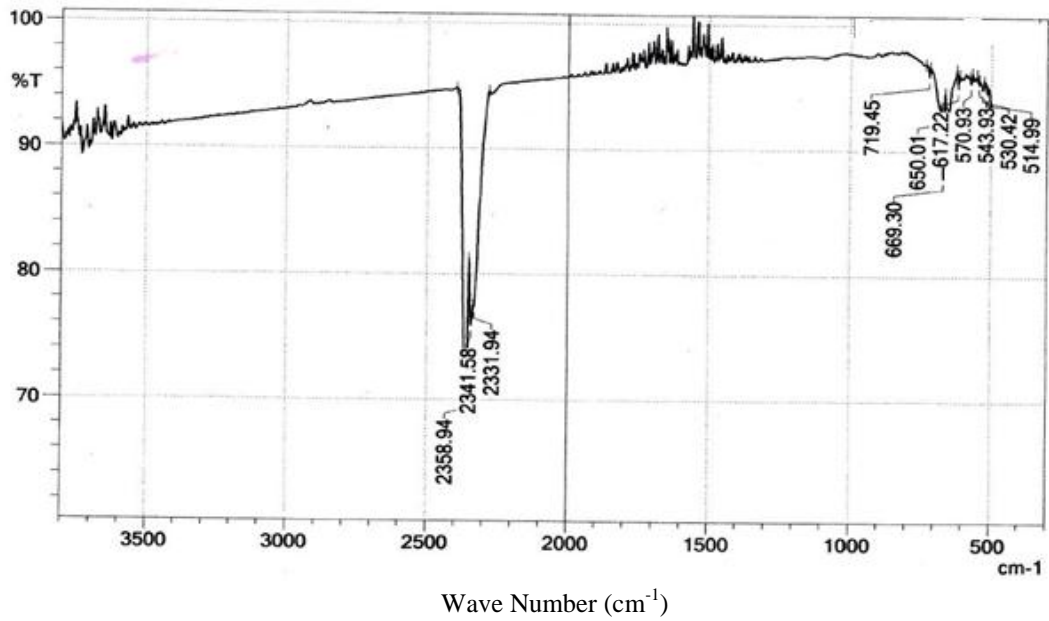


Figure 4.4: FTIR spectrum of $\text{Li}_{3.9}\text{Ti}_{4.9}\text{Cu}_{0.1}\text{Zn}_{0.1}\text{O}_{12}$

Table 4.1: FTIR data analysis for LTO

Serial no.	Peak position cm^{-1}				Comment
	Pure LTO ($\text{Li}_4\text{Ti}_5\text{O}_{12}$)	$\text{Li}_4\text{Ti}_{4.9}\text{Cu}_{0.05}\text{Zn}_{0.05}\text{O}_{12}$	$\text{Li}_{3.9}\text{Ti}_5\text{Cu}_{0.05}\text{Zn}_{0.05}\text{O}_{12}$	$\text{Li}_{3.9}\text{Ti}_{4.9}\text{Cu}_{0.1}\text{Zn}_{0.1}\text{O}_{12}$	
1	503.42	501.49	514.99	501.49	Stretching vibration of Ti-O-Ti bond
2	514.99	514.99	530.42	514.99	
3	532.35	545.85	543.93	530.2	
4	543.93	569.00	570.93	543.93	
5	555.50	607.58	617.22	609.51	
6	572.86	617.22	650.01	617.22	
7	597.93	650.01	669.30	650.01	
8	617.22	669.30	719.45	669.30	
9	2331.58	2331.94	2331.94	2331.94	Stretching vibration of Ti-O bond
10	2341.58	2341.58	2341.58	2341.58	
11	2360.87	2358.94	2358.94	2360.87	

4.2 XRD Spectra Analyses of Prepared LTO Based Materials

XRD spectrum of the prepared LTOs is presented from figure 4.7 to figure 4.10.

Investigation on the obtained diffractogram with ICDD card-00-009-0432 revealed that the pattern did not differ significantly from each other. However, the difference in peak broadening and peak intensity among the diffractogram indicate differences in crystallinity and crystallite size of the prepared LTOs. Prior to discussion of the result it is quite rational here to discuss some basic points regarding the structure of LTO.

It is well known that $\text{Li}_4\text{Ti}_5\text{O}_{12}$ possess a face-centered cubic spinel structure grounded on space group symmetry of $\text{Fd}\bar{3}\text{m}$. In the $\text{Li}_4\text{Ti}_5\text{O}_{12}$ spinel structure, tetrahedral 8a sites are completely taken up by Li and the octahedral 16d sites are arbitrarily occupied by Li and Ti with an atomic ratio of 1:5 in a cubic close-packed oxygen array. $\text{Li}_4\text{Ti}_5\text{O}_{12}$ can be defined as $[\text{Li}]_{8a}[\text{Ti}_{5/3}\text{Li}_{1/3}]_{16d}[\text{O}_4]_{32e}$. $\text{Li}_4\text{Ti}_5\text{O}_{12}$ is one of the culminated members of $\text{Li}_{3+x}\text{Ti}_{6-x}\text{O}_{12}$ ($0 \leq x \leq 1$) with $\text{Fd}\bar{3}\text{m}$ (space group) spinel structure [94] and lattice constant is 8.368, [95] 8.365 [96]. Lithium ions inhabit tetrahedral 8a site, and 1/6 of octahedral 16d sites, whereas the rest of octahedral sites were engaged by tetra valence Ti ions. Oxygen ions localize at 32e site. The structure can be demonstrated in Figure 4.5. The structure of the $\text{Li}_4\text{Ti}_5\text{O}_{12}$ can be formulated as

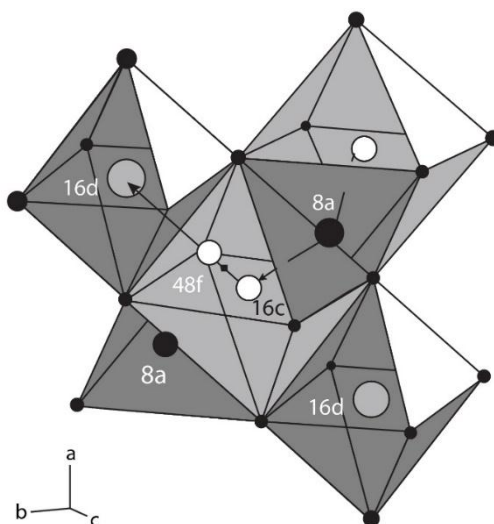
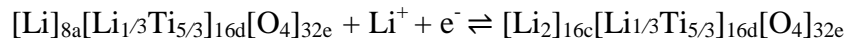


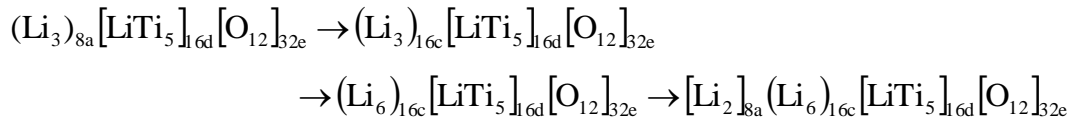
Figure 4.5: Crystal structure of spinel LTO with $\text{Fd}\bar{3}\text{m}$ space group. Black: Li^+ . Octahedron with 16d and 16c site share common edge 16d and 16c site share common faces with tetrahedron 48f. Lithium can transport through 8a site to 16c site and vice versa [97].

$\text{Li}_{3(8a)}[\text{LiTi}_5]_{16d}\text{O}_{12(32e)}$ [98], in which octahedral 16c sites and tetrahedral 8b and 48f sites are empty, which is appropriate for Li insertion and extraction [99,100]. $[\text{TiO}_6]$ is the core casing for Li insertion/extraction. There is no structural changes when less than 4.5 Li ions insert/extract in the casing during the charge/discharge route [101] by which LTO is also called zero-strain material, representing that it is an outstanding substantial in terms of cycle capacity performance as anode material for LIBs.

During the insertion of Li^+ , three Li atoms at 8a sites relocate to 16c sites, and the inserted three Li^+ move to 16c sites via 8a sites. Upon extraction, Li atoms are mined out from 16c sites via 8a sites, and the other Li atoms transfer back to 8a sites from 16c sites [99]. Assuring the stable $\text{Li}_4\text{Ti}_5\text{O}_{12}$ framework, the lattice parameters virtually retain unchanged throughout the process. This is most likely happened due to the Coulomb repulsion between nearest Li^+ lodging the 8a-16c sites separated by 1.81 Å [94]. At last, it changes into $\text{Li}_7\text{Ti}_5\text{O}_{12}$ ($[\text{Li}_2]_{16c}[\text{Ti}_{5/3}\text{Li}_{1/3}]_{16d}[\text{O}_4]_{32e}$), and three Ti^{4+} are reduced to Ti^{3+} [99]. The electrochemical reaction can be labeled as:



The structure changed equation can be described as following:



It is obvious that through lithium intercalation, spinel structure of $\text{Li}_4\text{Ti}_5\text{O}_{12}$ changes into a rock salt structure of $\text{Li}_7\text{Ti}_5\text{O}_{12}$ [102] as shown in Figure 4.6. The edge sharing

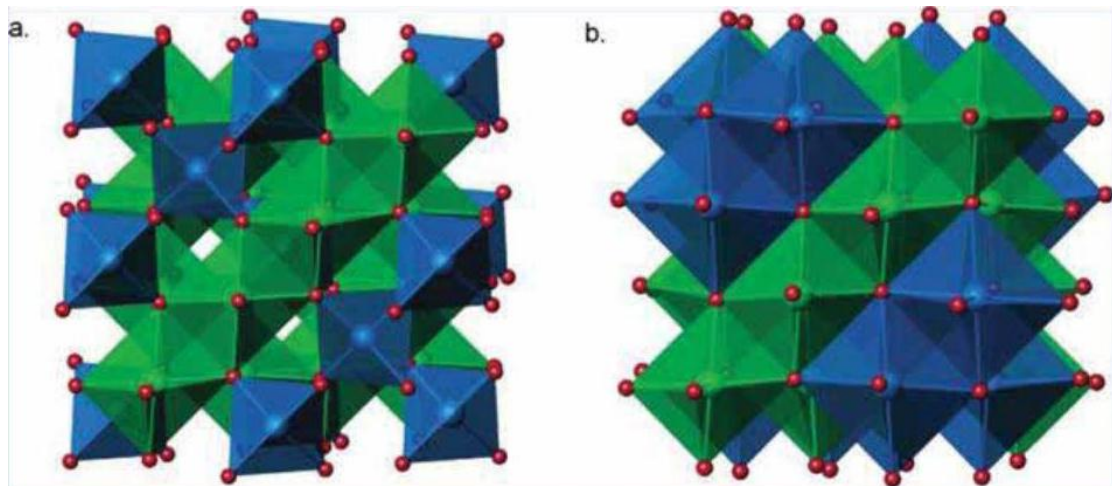


Figure 4.6: (a) $\text{Li}_4\text{Ti}_5\text{O}_{12}$ spinel structure type. Blue tetrahedra represent lithium, and green octahedra represent disordered lithium and titanium. (b)

Li₇Ti₅O₁₂, rock salt. Blue octahedra represent lithium, and green octahedra represent disordered lithium and titanium [102]

[Li_{1/6}Ti_{5/6}]O₆ octahedral form a three dimensional network that connects the 8a sites via the 16c sites presenting the most likely diffusion process for the Li⁺ in spinel structure [104]. Since the context of Li₄Ti₅O₁₂ is very robust, the lattice parameters remain almost unaffected upon Li insertion and extraction [97]. While more than 3 Li per unit intercalates into Li₄Ti₅O₁₂ the additional 2 Li instigated to inhabit the empty tetrahedral 8a site with descending voltage to 0.01 V [105,106].

In this thesis, the structure and phase composition of the prepared LTOs were investigated by XRD pattern. Obtained spectra were analyzed and compared with the standard results. Spectrum of pure LTO and Cu & Zn co-doped LTOs are shown in Figure 4.7-4.10. From figure 4.7 it is seen that the characteristic diffraction peaks at 2θ of 18.3, 35.58, 43.2449, 43.1, 57.2065, 62.8447 and 66.1006 correspond to the planes (111), (311), (400), (333), (440) and (531) respectively which are well fitted to the spinel LTO phase. The diffraction pattern are in adequate agreement with JCPDS (No. 26-1198) indicating the face centered cubic spinel structure with Fd3m space group [107] Figure 4.8 – 4.10 represent the X-ray diffraction pattern of Li₄Ti_{4.9}Cu_{0.05}Zn_{0.05}O₁₂, Li_{3.9}Ti₅Cu_{0.05}Zn_{0.05}O₁₂ and Li_{3.9}Ti_{4.9}Cu_{0.1}Zn_{0.1}O₁₂ and no significant shift was observed in the diffraction peaks. The lattice parameter values were calculated for Li₄Ti₅O₁₂, Li₄Ti_{4.9}Cu_{0.05}Zn_{0.05}O₁₂, Li_{3.9}Ti₅Cu_{0.05}Zn_{0.05}O₁₂ and Li_{3.9}Ti_{4.9}Cu_{0.1}Zn_{0.1}O₁₂ and the values are 8.3692 Å, 8.3742 Å, 8.3834 Å and 8.3709 Å, respectively. It is to be mentioned here that the lattice parameter values were calculated using the following equation 4.1:

$$d = \frac{a}{\sqrt{h^2 + l^2 + k^2}} \text{ ----- (4.1)}$$

where, d = interplaner distance (Å); h, l & k are miller indices and a is lattice parameter.

The calculated lattice parameter values of the prepared LTOs have a good agreement with the results of [95, 96]. It can be concluded from the XRD spectrum that both pure Li₄Ti₅O₁₂ and Cu & Zn co-doped LTOs showed peaks representing single phase of spinel lithium titanium oxide (cubic phase, space group Fd-3m) which exactly match with standard peaks of spinel Li₄Ti₅O₁₂. Thus it can be concluded that the anode materials were successfully prepared and well crystallized by calcining

precursor at temperature of 750 °C. XRD spectra of all prepared LTOs are given below in the enlarge form.

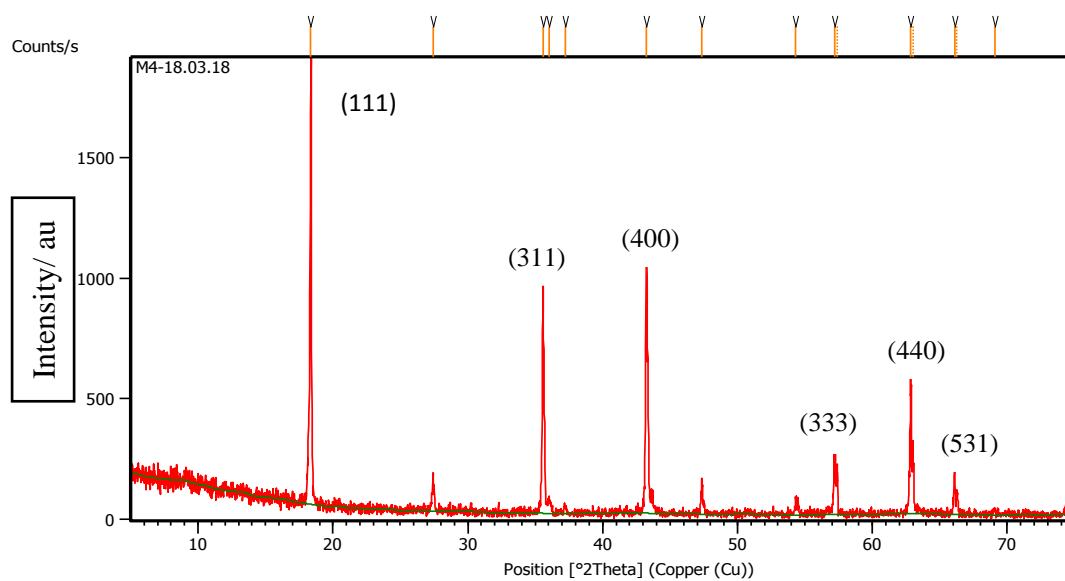


Figure 4.7: XRD spectrum of pure $\text{Li}_4\text{Ti}_5\text{O}_{12}$

Table 4.2.: List of important peaks of the prepared $\text{Li}_4\text{Ti}_5\text{O}_{12}$

No.	h	k	l	d-spacing [Å]	2 Theta [deg]
1	1	1	1	4.83196	18.3615
2	3	1	1	2.52292	35.5853
3	4	0	0	2.09216	43.2449
4	3	3	3	1.60901	57.2065
5	4	4	0	1.47753	62.8447
6	5	3	1	1.41242	66.1006

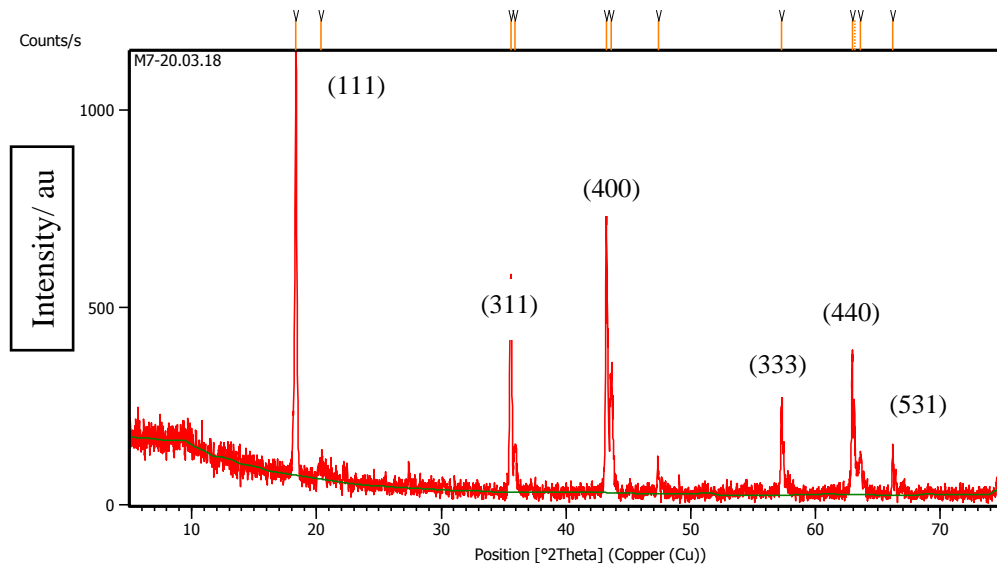


Figure 4.8: XRD spectrum of Zn & Cu co-doped $\text{Li}_4\text{Ti}_{4.9}\text{Cu}_{0.05}\text{Zn}_{0.05}\text{O}_{12}$

Table 4.3: List of important peaks of the prepared $\text{Li}_4\text{Ti}_{4.9}\text{Cu}_{0.05}\text{Zn}_{0.05}\text{O}_{12}$

No.	h	k	l	d-spacing [\AA]	2 Theta [deg]
1	1	1	1	4.83486	18.3504
2	3	1	1	2.52385	35.5718
3	4	0	0	2.09235	43.2408
4	3	3	3	1.60828	57.2864
5	4	4	0	1.47559	62.9369
6	5	3	1	1.41083	66.1845

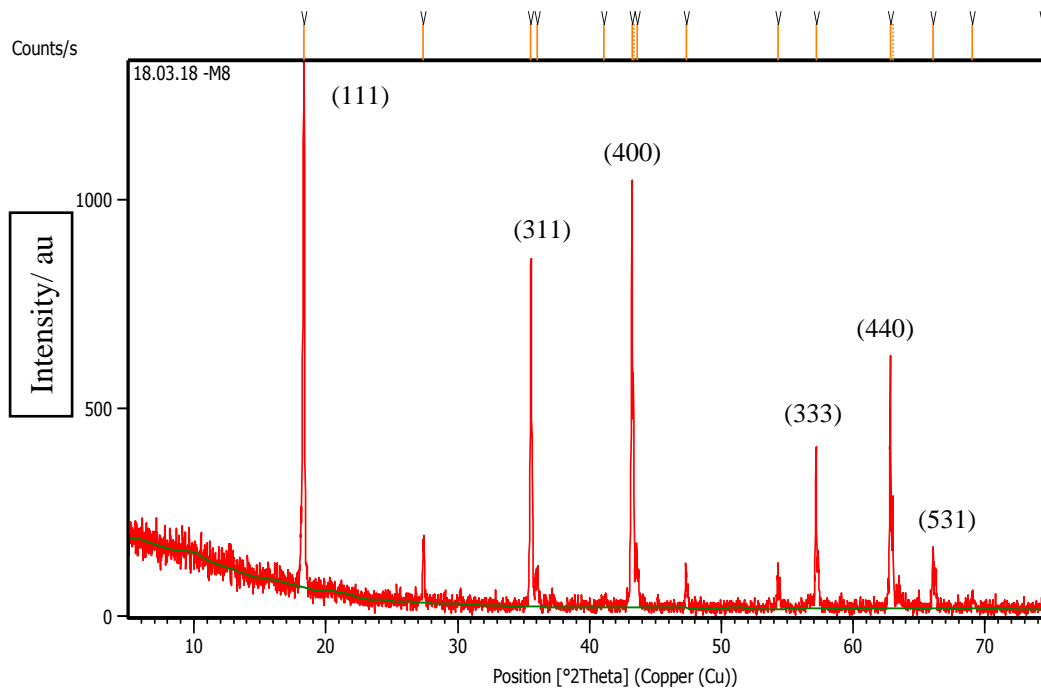


Figure 4.9: XRD spectrum of Zn & Cu co-doped $\text{Li}_{3.9}\text{Ti}_5\text{Cu}_{0.05}\text{Zn}_{0.05}\text{O}_{12}$

Table 4.4: List of important peaks of the prepared $\text{Li}_{3.9}\text{Ti}_5\text{Cu}_{0.05}\text{Zn}_{0.05}\text{O}_{12}$

No.	h	k	l	d-spacing [Å]	2 Theta [deg]
1	1	1	1	4.83299	18.3576
2	3	1	1	2.52404	35.5689
3	4	0	0	2.09099	43.2326
4	3	3	3	1.60960	57.1836
5	4	4	0	1.47848	62.7996
6	5	3	1	1.41338	66.0501

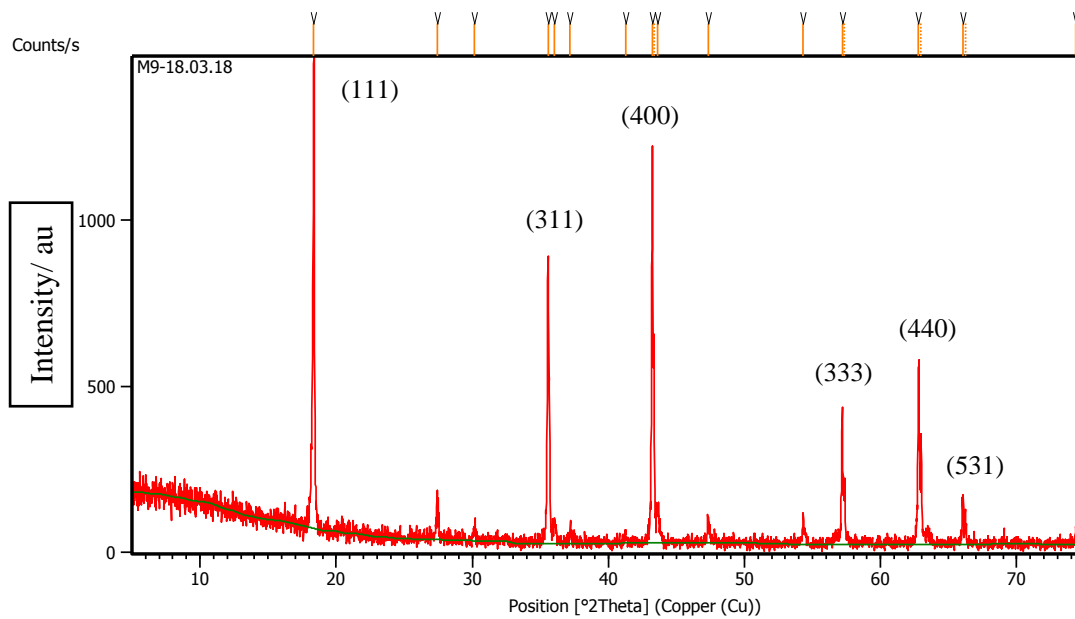


Figure 4.10: XRD spectrum of Zn & Cu co-doped $\text{Li}_{3.9}\text{Ti}_{4.9}\text{Cu}_{0.1}\text{Zn}_{0.1}\text{O}_{12}$

Table 4.5: List of important peaks of the prepared $\text{Li}_{3.9}\text{Ti}_{4.9}\text{Cu}_{0.1}\text{Zn}_{0.1}\text{O}_{12}$

No.	h	k	l	d-spacing [Å]	2 Theta [deg]
1	1	1	1	4.83196	18.3615
2	3	1	1	2.52292	35.5853
3	4	0	0	2.09216	43.2449
4	3	3	3	1.60901	57.2065
5	4	4	0	1.47753	62.8447
6	5	3	1	1.41242	66.1006

4.3 SEM Spectra Analyses of Prepared LTO Based Materials

Figure 4.11 to figure 4.14 represent the SEM photographs of prepared pure LTO ($\text{Li}_4\text{Ti}_5\text{O}_{12}$), $\text{Li}_4\text{Ti}_{4.9}\text{Cu}_{0.05}\text{Zn}_{0.05}\text{O}_{12}$, $\text{Li}_{3.9}\text{Ti}_5\text{Cu}_{0.05}\text{Zn}_{0.05}\text{O}_{12}$ and $\text{Li}_{3.9}\text{Ti}_{4.9}\text{Cu}_{0.1}\text{Zn}_{0.1}\text{O}_{12}$. The SEM photograph provides the particle size (one side length). It is seen from the photographs that all the prepared LTOs possess chips like shape. The morphologies of all prepared LTOs are almost same. No significant change happened in the morphologies due to the co-doping of different ratio of Cu & Zn into $\text{Li}_4\text{Ti}_5\text{O}_{12}$ that can be correspond to the X-ray diffraction result all are single phase of spinel lithium titanium oxide. From this observation, it is clear that the co-doping of Cu and Zn dopant in the $\text{Li}_4\text{Ti}_5\text{O}_{12}$ no morphological change happened.

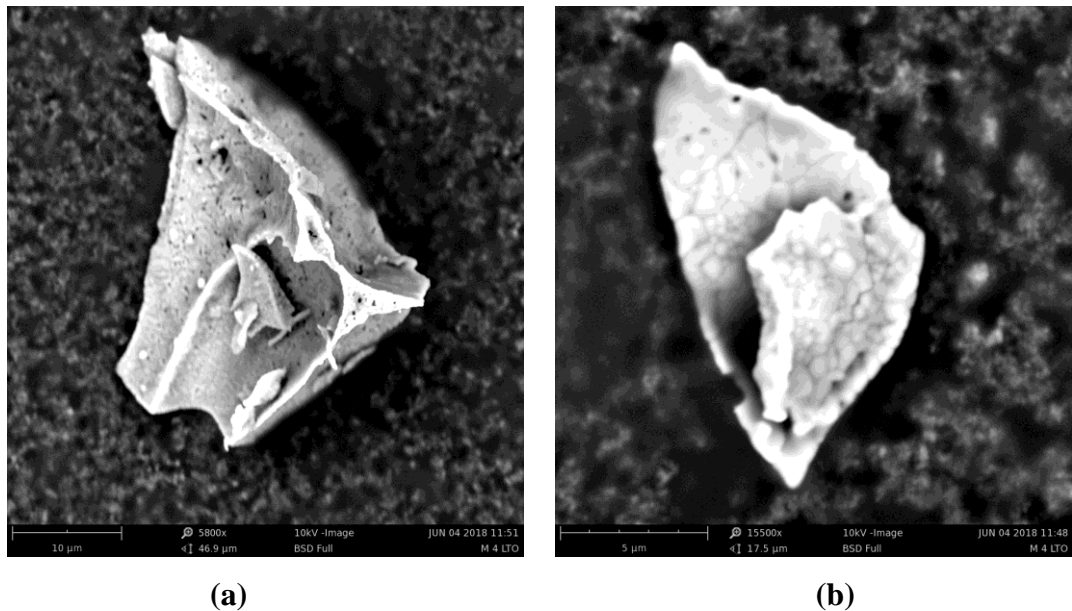
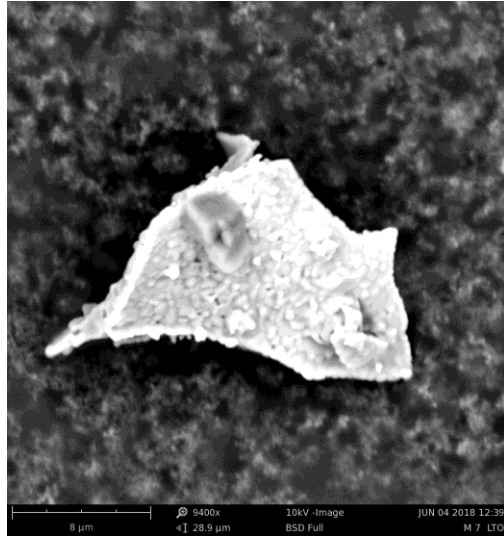


Figure 4.11: SEM image of pure $\text{Li}_4\text{Ti}_5\text{O}_{12}$ at different magnifications



(a)

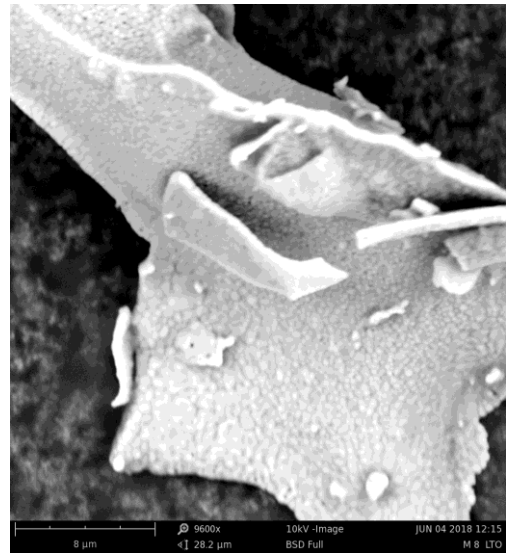


(b)

Figure 4.12: SEM image of Cu and Zn doped $\text{Li}_4\text{Ti}_{4.9}\text{Cu}_{0.05}\text{Zn}_{0.05}\text{O}_{12}$ (LTO) at different magnifications



(a)



(b)

Figure 4.13: SEM image of Cu and Zn doped $\text{Li}_{3.9}\text{Ti}_5\text{Cu}_{0.05}\text{Zn}_{0.05}\text{O}_{12}$ (LTO) at different magnifications

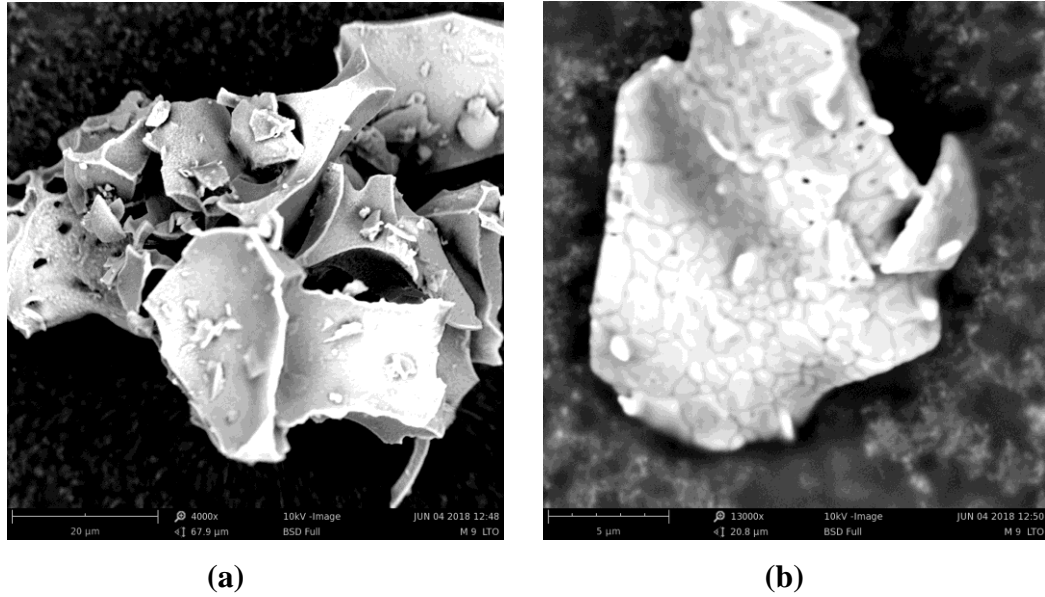


Figure 4.14: SEM image of Cu and Zn doped $\text{Li}_{3.9}\text{Ti}_{4.9}\text{Cu}_{0.1}\text{Zn}_{0.1}\text{O}_{12}$ (LTO) at different magnifications

4.4 Prepared LTO Based Materials Electrochemical Works

Prepared LTO based materials were used to fabricate a handmade coin cell lithium ion battery. Anode materials were mixed with acetylene black as conducting agent, and polyvinylidene fluoride (PVDF) as binder in N-methylpyrrolidone (NMP). The blended slurries were pasted onto an aluminum foil and dried in oven to fabricate the electrode. In the cell 1M LiPF_6 electrolyte was used in solvent in a 1:1:1 (vol%) mixture of ethylene carbonate, ethyl methyl carbonate and dimethyl carbonate as shown in figure 4.15.



Figure 4.15: Fabricated cell

Finally, the test cells were assembled using Li foil as cathode and polypropylene film as the separator. Here in the experiment one serious drawback happened

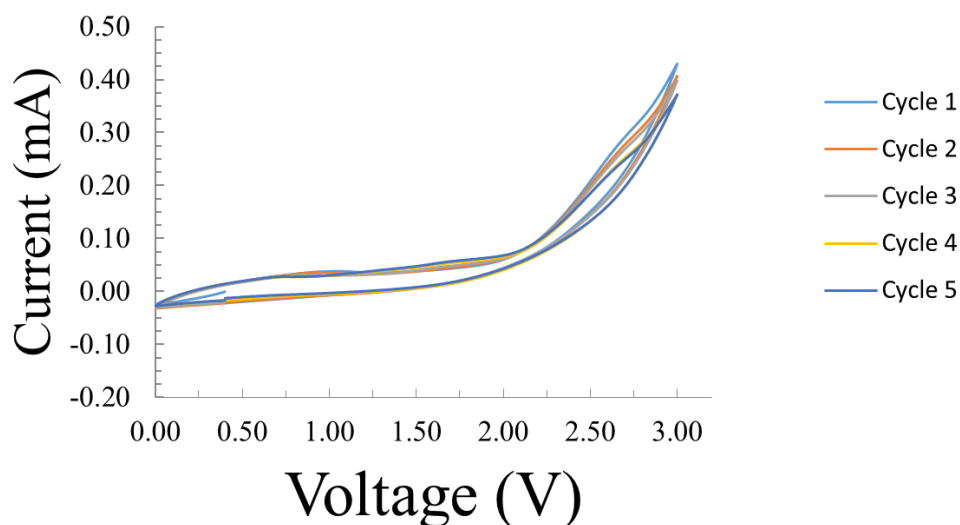


Figure 4.16: Cyclic voltammetry of the fabricated cell

which is to be mentioned. Fabrication of the cell was done in a semi-closed polyethene chamber which was not fully evacuated. In presence of controlled atmospheric condition it was done where restricted amount of oxygen, water vapor, hydrogen were present. In this situation may be most of the lithium foil has been converted into lithium oxide. Moreover, an attempt has been performed to do an electrochemical work. Although the result is not satisfactory but from the CV as shown in figure 4.16 it can be told that prepared LTOs are conductive and can be used as anode material in lithium ion battery.

Chapter – V

Conclusion

LTO based anode materials have been prepared by sol-gel method where Cu and Zn as dopant into $\text{Li}_4\text{Ti}_5\text{O}_{12}$ for lithium ion battery. Either Li or Ti or both have been replaced by Cu and Zn by co-doping into $\text{Li}_4\text{Ti}_5\text{O}_{12}$ to enhance the conductivity. Spectroscopic techniques, such as Fourier-Transform Infrared Spectroscopy (FTIR), scanning electron microscopy (SEM), (EDX) and X-ray diffraction (XRD) are used for the characterization of morphology, particle size and crystal structure of the prepared LTO based anode materials.

IR spectra below 800 cm^{-1} confirm symmetric stretching vibrations of Ti-O bonds of TiO_6 octahedron in prepared LTOs. Stretching bands of Ti-O-Ti bonds at around 2360.87 , 2341.58 and 2331.94 cm^{-1} also confirm LTOs formation. XRD spectra that both pure $\text{Li}_4\text{Ti}_5\text{O}_{12}$ and Cu & Zn co-doped LTOs showed peaks representing single phase of spinel lithium titanium oxide (cubic phase, space group Fd-3m) which are in good agreement with Joint Committee on Powder Diffraction Standards, JCPDS (No. 26-1198) data. SEM photographs of prepared pure LTO ($\text{Li}_4\text{Ti}_5\text{O}_{12}$), $\text{Li}_4\text{Ti}_{4.9}\text{Cu}_{0.05}\text{Zn}_{0.05}\text{O}_{12}$, $\text{Li}_{3.9}\text{Ti}_5\text{Cu}_{0.05}\text{Zn}_{0.05}\text{O}_{12}$ and $\text{Li}_{3.9}\text{Ti}_{4.9}\text{Cu}_{0.1}\text{Zn}_{0.1}\text{O}_{12}$ possess chips like shape. The morphologies of all prepared LTOs are almost same that correspond the X-ray diffraction result. From the electrochemical experiment it can be tell that prepared LTOs are conductive and can be used as anode material in lithium ion battery.

References

1. Armand, M. and Tarascon, J. M., 2008, "Building better batteries," *Nature*, Vol. 451, pp. 652-657
2. Whittingham, M. S. (1976). "Electrical Energy Storage and Intercalation Chemistry". *Science*. Vol. 192(4244), pp. 1126–1127
3. Landi, B. J., 2009, "Carbon nanotubes for lithium ion batteries," *Energy Environ. Sci.*, Vol. 2, pp. 638-654
4. *Handbook of Batteries*, 3 ed.: McGraw-Hill, 2002
5. Fergus, J. W., 2010, "Recent developments in cathode materials for lithium ion batteries", *Journal of Power Sources*, Vol. 195, pp. 939-954
6. Rao, B. M. L., 1977, "Lithium-Aluminum electrode," *Journal of Electrochemical Society*, Vol. 124, pp. 1490-1492
7. Huang, S., Wen, Z., Zhu, X. and Lin, Z., 2007, *Journal of Power Sources*, Vol. 165, p. 408
8. Edwards, P. P., Egdell, R. G., Fragala, I., Goodenough, J. B., Harrison, M. R., Orchard, A. F. and Scott, E. G., 1984, *Journal of Solid State Chemistry*, Vol. 54, p. 127
9. Dahn, J. R. and Haering, R. R., 1989, *Journal of Power Sources*, Vol. 26, p. 397
10. Xu, K., 2008, "Tailoring electrolyte composition for LiBOB," *Journal of Electrochemical Society*, Vol. 155, pp. A733-738
11. Aurbach, D., et al., 2004, "Design of electrolyte solutions for Li and Li-Ion batteries: A review," *Electro Chemical Acta*, Vol. 50, pp. 247-254
12. Vetter, J., Novak, P., Wagner, M. R., Veit, C., Moller, K. C., Besenhard, J. O., Winter, M., Wohlfahrt-Mehrens, M., Vogler, C. and Hammouche, A., 2005, "Ageing mechanisms in lithium-ion batteries", *Journal of Power Sources*, Vol. 147, (1-2), pp. 269-281
13. Zhang, W. J., 2011, "A review of the electrochemical performance of alloy anodes for lithium-ion batteries", *Journal of Power Sources*, Vol. 196, (1), pp. 13-24
14. Gao, X. P., Bao, J. L., Pan, G. L., Zhu, H. Y., Huang, P. X., Wu, F. and Song, D. Y., 2004, "Preparation and electrochemical performance of polycrystalline and

- single crystalline CuO nanorods as anode materials for Li ion battery”, *Journal of Physical Chemistry B*, Vol. 108, (18), pp. 5547-5551
15. Zhu, G. N., Wang, Y. G. and Xia, Y. Y., 2012, “Ti-based compounds as anode materials for Li-ion batteries”, *Energy & Environmental Science*, Vol. 5, (5), pp. 6652-6667
 16. Ferg, E., Gummow, R. J., de Kock, A. and Thackeray, M. M., 1994, “Spinel Anodes for Lithium-Ion Batteries”, *Journal of The Electrochemical Society*, Vol. 141, (11), pp. L147-L150
 17. Ouyang, C. Y., Zhong, Z. Y. and Lei, M. S., 2007, “Ab initio studies of structural and electronic properties of $\text{Li}_4\text{Ti}_5\text{O}_{12}$ spinel”, *Electrochemistry Communications*, Vol.9, (5), pp. 1107-1112
 18. Ohzuku, T., Ueda, A. and Yamamoto, N., 1995, “Zero-strain insertion material of $\text{Li}[\text{Li}_{1/3}\text{Ti}_{5/3}]\text{O}_4$ for rechargeable lithium cells”, *Journal of the Electrochemical Society*, Vol. 142, (5), pp.1431-1435
 19. Kavan, L. and Grätzel, M., 2002, “Facile synthesis of nanocrystalline $\text{Li}_4\text{Ti}_5\text{O}_{12}$ (Spinel) exhibiting fast Li insertion”, *Electrochemical and Solid-State Letters*, Vol. 5 (2), pp. A39-A42
 20. Colin, J. F., Godbole, V. and Novák, P., 2010, “In-situ neutron diffraction study of Li insertion in $\text{Li}_4\text{Ti}_5\text{O}_{12}$ ”, *Electrochemistry Communications*, Vol.12 (6), pp. 804-807
 21. Ma, J., Wang, C. and Wroblewski, S., 2007, “Kinetic characteristics of mixed conductive electrodes for lithium ion batteries”, *Journal of Power Sources*, Vol. 164 (2), pp. 849-856
 22. Yao, X., Xie, S., Nian, H. and Chen, C., 2008, “Spinel $\text{Li}_4\text{Ti}_5\text{O}_{12}$ as a reversible anode material down to 0 V”, *Journal of Alloys and Compounds*, Vol.465 (1), pp. 375-379
 23. Roberts, M. R., Vitins, G. and Owen, J. R., 2008, “High-throughput studies of $\text{Li}_{1-x}\text{Mg}_{x/2}\text{FePO}_4$ and $\text{LiFe}_{1-y}\text{Mg}_y\text{PO}_4$ and the effect of carbon coating”, *Journal of Power Sources*, Vol. 179 (2), pp. 754-762
 24. Goodenough, J. B. and Kim, Y., 2009, “Challenges for rechargeable Li batteries”, *Chemistry of Materials*, Vol. 22 (3), pp. 587-603
 25. Wakihara, M., 2001, “Recent developments in lithium ion batteries”, *Materials Science and Engineering: R: Reports*, Vol. 33 (4), pp. 109-134

26. Tarascon, J. M. and Armand, M., 2001, "Issues and challenges facing rechargeable lithium batteries", *Nature*, Vol. 414 (6861), pp. 359-367
27. Wakihara, M., 2001, "Recent developments in lithium ion batteries", *Materials Science and Engineering: R: Reports*, Vol. 33 (4), pp. 109-134
28. Dunn, B., Kamath, H. and Tarascon, J. M., 2011, "Electrical energy storage for the grid: A battery of choices", *Science*, Vol. 334 (6058), pp.928-935
29. Whittingham, M. S., 2004, "Lithium batteries and cathode materials", *Chemical Reviews-Columbus*, Vol. 104(10), pp. 4271-4302
30. Chebiam, R., Prado, F. and Manthiram, A., 2001, "Soft Chemistry Synthesis and Characterization of Layered $\text{Li}_{1-x}\text{Ni}_{1-y}\text{Co}_y\text{O}_{2-\delta}$ ($0 \leq x \leq 1$ and $0 \leq y \leq 1$)", *Journal of Materials Chemistry*, Vol. 13(9), pp. 2951-2957
31. Armstrong, A. R. and Bruce, P. G., 1996, "Synthesis of layered LiMnO_2 as an electrode for rechargeable lithium batteries", *Nature*, Vol. 381(6582), pp. 499-500
32. Reed, J., Ceder, G. and Ven A. V. D., 2001, "Layered-to-spinel phase transition in Li_xMnO_2 ", *Electro chemical and Solid State Letters*, Vol. 4(6) pp. A78-A81
33. Jang, D. H., Shin, Y. J. and Oh S. M., 1996, "Dissolution of spinel oxides and capacity losses in 4 V $\text{Li}/\text{Li}_x\text{Mn}_2\text{O}_4$ cells", *Journal of the Electrochemical Society*, Vol. 143(7), pp. 2204-2211
34. Ngala, J. K., Chernova, N. A., Ma, M., Mamak, M., Zavalij, P. Y. and Whittingham, M. S., 2004, "The synthesis, characterization and electrochemical behavior of the layered $\text{LiNi}_{0.4}\text{Mn}_{0.4}\text{Co}_{0.2}\text{O}_2$ compound", *Journal of Materials Chemistry*, Vol. 14(2), pp. 214-220
35. Park, K., Son, J., Chung, H., Kim, S., Lee, C. and Kim, H., 2003, "Synthesis of LiFePO_4 by co-precipitation and microwave heating", *Electrochemistry Communications*, Vol. 5(10), pp. 839-842
36. Zhang, Z. J. and Ramadass, P., 2013, "Lithium-ion battery systems and technology. Batteries for sustainability", Springer, pp. 319-357
37. Loeffler, N., Bresser, D. and Passerini, S., 2015, "Secondary lithium-ion battery anodes: From first commercial batteries to recent research activities", *Johnson Matthey Technology Review*, Vol. 59(1), pp. 34-44

38. Kumar, T. P., Kumari, T. S. D. and Stephan, A. M., 2009, "Carbonaceous anode materials for lithium-ion batteries-the road ahead", *Journal of the Indian Institute of Science*, Vol. 89(4), pp. 393-424
39. Scrosati, B. and Garche, J., 2010, "Lithium batteries: Status, prospects and future", *Journal of Power Sources*, Vol. 195(9), pp. 2419-2430
40. Lou, X. W., Wang, Y., Yuan, C., Lee, J. Y. and Archer, L. A., 2006, "Template free synthesis of SnO₂ hollow nanostructures with high lithium storage capacity", *Advanced Materials*, Vol. 18(17), pp. 2325-2329
41. Paek, S. M., Yoo, E. J. and Honma, I., 2008, "Enhanced cyclic performance and lithium storage capacity of SnO₂/graphene nanoporous electrodes with three-dimensionally delaminated flexible structure", *Nano Lett.*, Vol. 9(1), pp. 72-75
42. Zhang, B., Zheng, Q. B., Huang, Z. D., Oh, S.W. and Kim, J. K., 2011, "SnO₂-graphene-carbonnanotube mixture for anode material with improved rate capacities", *Carbon*, Vol. 49(13), pp. 4524-4534
43. Sato, K., Noguchi, M., Demachi, A., Oki, N. and Endo, M. A., 1994, "Mechanism of lithium storage in disordered carbons", *Science*, Vol. 264(5158), pp. 556-558
44. Uthaisar, C. and Barone. V., 2010, "Edge effects on the characteristics of Li diffusion in grapheme", *Nano Letter*, Vol. 10(8), pp. 2838-2842
45. Hsieh, C. T. and Lin J. Y., 2010, "Influence of Li addition on charge/discharge behavior of spinel lithium titanate", *Journal of Alloys and Compounds*, Vol. 506, pp. 231-236
46. Shen, C. M., Zhang, X. G., Zhou, Y. K. and Li, H. L., 2003, "Preparation and characterization of nanocrystalline Li₄Ti₅O₁₂ by sol-gel method", *Materials Chemistry and Physics*, Vol. 78, pp. 437-441
47. Hao, Y. J., Lai, Q. Y., Lu, J. Z., Liu, D. Q. and Ji, X. Y., 2007, "Influence of various complex agents on electrochemical property of Li₄Ti₅O₁₂ anode material", *Journal of Alloys and Compounds*, Vol. 439, pp. 330-336
48. Kim, D. H., Ahn, Y. S. and Kim, J., 2005, "Polyol-mediated synthesis of Li₄Ti₅O₁₂ nanoparticle and its electrochemical properties", *Electrochemical Communication.*, Vol. 7, pp. 1340-1344

49. Lee, S. C., Lee, S. M., Lee, J. W., Lee, J. B., Han, S. S., Lee, H. C. and Kim, H. J., 2009, "Spinel $\text{Li}_4\text{Ti}_5\text{O}_{12}$ nanotubes for energy storage materials", *Journal of Physical Chemistry C*, Vol. 113, pp. 18420–18423
50. Tang, Y., Yang, L., Qiu, Z. and Huang, J., 2009, "Template-free synthesis of mesoporous spinel lithium titanate microspheres and their application in high-rate lithium ion batteries", *Journal of Material Chemistry*, Vol. 19, pp. 5980-5984
51. Sorensen, E. M., Barry, S. J., Jung, H. K., Rondinelli, J. R., Vaughey, J. T. and Poeppelmeier, K. R., 2006, "Three-dimensionally ordered macroporous $\text{Li}_4\text{Ti}_5\text{O}_{12}$: effect of wall structure on electrochemical properties", *Chemistry of Materials*, Vol. 18, p. 482
52. He, N., Wang, B. and Huang, J., 2010, "Preparation and electrochemical performance of mono disperse $\text{Li}_4\text{Ti}_5\text{O}_{12}$ hollow spheres", *Journal of Solid State Electrochemistry*, Vol. 14, pp. 1241–1246
53. Lu, H. W., Zeng, W., Li, Y. S. and Fu, Z. W., 2007, "Fabrication and electrochemical properties of three-dimensional net architectures of anatase TiO_2 and spinel $\text{Li}_4\text{Ti}_5\text{O}_{12}$ nanofibers", *Journal of Power Sources*, Vol. 164, pp. 874-879
54. Ju, S. H. and Kang, Y. C., 2009, "Effects of preparation conditions on the electrochemical and morphological characteristics of $\text{Li}_4\text{Ti}_5\text{O}_{12}$ powders prepared by spray pyrolysis", *Journal of Power Sources*, Vol. 189, pp. 185-190
55. Bai, Y., Wang, F., Wu, F., Wu, C. and Bao, L.Y., 2008, "Influence of composite LiCl-KCl molten salt on microstructure and electrochemical performance of spinel $\text{Li}_4\text{Ti}_5\text{O}_{12}$ ", *Electrochemical Acta*, Vol. 54, pp. 322-327
56. Mohammadi, M. R. and Fray, D. J., 2010, "Low temperature nano structured lithium titanates: controlling the phase composition, crystal structure and surface area", *Journal of Sol-Gel Science and Technology*, Vol. 55, pp. 19
57. Kim, H. J., Oh, M. H., Son, W. K., Kim, T. I. and Park, S. G., "Novel synthesis method and electrochemical characteristics of lithium titanium oxide as anode material for high power device presented at properties and applications of dielectric materials", 8th International Conference on, 2006

58. Alias, N., Kufian, M., Teo, L., Majid, S. and Arof, A., 2009, "Synthesis and characterization of $\text{Li}_4\text{Ti}_5\text{O}_{12}$ ", *Journal of Alloys and Compounds*, Vol. 486, pp. 645-648
59. Hao, Y., Lai, Q., Xu, Z., Liu, X. and Ji, X., 2005, "Synthesis by TEA sol-gel method and electrochemical properties of $\text{Li}_4\text{Ti}_5\text{O}_{12}$ anode material for lithium-ion battery", *Solid State Ionics*, Vol. 176, pp. 1201-1206
60. Thackeray, M. M., Wolverton, C. and Isaacs, E. D., 2012, "Electrical energy storage for transportation - approaching the limits of, and going beyond, lithium-ion batteries", *Energy Environmental Science*. Vol. 5(7) pp. 7854-7863
61. Teki, R., Datta, M. K., Krishnan, R., Parker, T. C., Lu, T. M. and Kumta, P. N., 2009, "Nanostructured silicon anodes for lithium ion rechargeable batteries", *Small*, Vol. 5(20) pp. 2236-2242
62. Zhang, L., in *Encyclopedia of Materials: Science and Technology*, (Eds: K. H. J. Buschow, W. C. Robert, C. F. Merton, I. Bernard, J. K. Edward, M. Subhash, V. Patrick), 2001, Elsevier, Oxford, 463
63. Belharouak, I. and Amine, K., 2003, " $\text{Li}_2\text{MTi}_6\text{O}_{14}$ (M=Sr, Ba): new anodes for lithium-ion batteries", *Electrochemistry Communications*, Vol. 5, pp. 435
64. Borghols, W. J. H., Wagemaker, M., Lafont, U., Kelder, E. M. and Mulder, F. M., 2009, "Size effects in the $\text{Li}_{4+x}\text{Ti}_5\text{O}_{12}$ spinel", *Journal of the American Chemical Society*, Vol. 131, pp. 17786-17792
65. Makimura, Y. and Ohzuku, T., 2009, "Investigation of ramsdellite titanates as possible new negative electrode materials for Li batteries", in *Encyclopedia of Electrochemical Power Sources*, (Eds: x00Fc, G. rgen), Elsevier, Amsterdam, 249
66. Wen, Z., Huang, S., Yang, X. and Lin, B., 2008, "Carbons for electrochemical energy storage and conversion systems", *Solid State Ionics*, Vol. 179, p.1800
67. Yi, T. F., Shu, J., Zhu, Y. R., Zhu, X. D., Zhu, R. S. and Zhou, A. N., 2010, "Ultrathin atomic layer deposited ZrO_2 coating to enhance the electrochemical performance of $\text{Li}_4\text{Ti}_5\text{O}_{12}$ as an anode material", *Journal of Power Sources*, Vol. 195, pp. 285
68. Kim, S. H., Park, H., Jee, S. H., Ahn, H. S., Kim, D. J., Choi, J. W., Yoon, S. J. and Yoon, Y. S., 2009, "Synthesis and structural properties of lithium titanium

- oxide powder as-synthesized by two step calcination process”, Korean Journal of Chemical Engineering, Vol. 26, p. 485
69. Jiang, C., Zhou, Y., Honma, I., Kudo, T. and Zhou, H., 2007, “Preparation and rate capability of $\text{Li}_4\text{Ti}_5\text{O}_{12}$ hollow-sphere anode material”, Journal of Power Sources, Vol. 166, pp. 514-518
 70. Li, J. R., Tang, Z. L., Luo, S. H., Lu, J. B. and Zhang, Z. T., 2007, “Effects of Li/Ti ratios on the electrochemical properties of $\text{Li}_4\text{Ti}_5\text{O}_{12}$ examined by time-resolved X-ray diffraction”, Research Gate, Vol. 336-338 I, p. 513
 71. Leonidov, I., Leonidova, O., Perelyaeva, L., Samigullina, R., Kovyazina, S. and Patrakeev, M. 200, “Structure, ionic conduction, and phase transformations in lithium titanate $\text{Li}_4\text{Ti}_5\text{O}_{12}$ ”, Physics of the Solid State, Vol. 45, pp. 2183-2188
 72. Pasquier, A. D., Plitz, I., Gural, J., Badway, F. and Amatucci, G. G., 2004, “Power-ion battery: bridging the gap between Li-ion and super capacitor chemistries”, Journal of Power Sources, Vol. 136, pp. 160-170
 73. Thackeray, M. M., 1995, “Structural considerations of layered and spinel lithiated oxides for lithium ion batteries”, Journal of the Electrochemical Society, Vol. 142, p. 2558
 74. Xiang, H. F., Zhang, X., Jin, Q. Y., Zhang, C. P., Chen, C. H. and Ge, X. W., 2008, “Effect of capacity matchup in the $\text{LiNi}_{0.5}\text{Mn}_{1.5}\text{O}_4/\text{Li}_4\text{Ti}_5\text{O}_{12}$ cells”, Journal of Power Sources, Vol. 183, pp. 355-360
 75. Liu, D. Q., Liu, X. Q. and He, Z. Z., 2007, “The elevated temperature performance of LiMn_2O_4 coated with $\text{Li}_4\text{Ti}_5\text{O}_{12}$ for lithium ion battery”, Materials Chemistry and Physics, Vol. 105, pp. 362-366
 76. Yi, T. F., Shu, J., Zhu, Y. R., Zhou, A. N. and Zhu, R. S., 2009, “Structure and electrochemical performance of $\text{Li}_4\text{Ti}_5\text{O}_{12}$ -coated $\text{LiMn}_{1.4}\text{Ni}_{0.4}\text{Cr}_{0.2}\text{O}_4$ spinel as 5 V materials”, Electrochemistry Communications, Vol. 11, pp. 91-94
 77. Capsoni, D., Bini, M., Massarotti, V., Mustarelli, P., Chiodelli, G., Azzoni, C. B., Mozzati, M. C., Linati, L. and Ferrari, S., 2008, “ ^1H chemical shifts in nonaxial, paramagnetic chromium (III) complexes”, Chemical Materials, Vol. 20, p. 4291
 78. Jovic, N., Antic, B., Kremenovic, A., Spasojevic-de B. A. and Spasojevic, V., 2003, “Cation ordering and order-disorder phase transition in Co substituted $\text{Li}_4\text{Ti}_5\text{O}_{12}$ spinels”, Physical Status Solidi, Vol. 18 p. 198

79. Wang, Y., Liu, H., Wang, K., Eiji, H. and Zhou, H., 2009, "The volume holographic optical storage potential in azo benzene containing polymers", *Journal of Materials Chemistry*, Vol. 19, p. 6789
80. Huang, S., Wen, Z., Lin, B., Han, J. and Xu, X., 2008, "The high-rate performance of the newly designed $\text{Li}_4\text{Ti}_5\text{O}_{12}/\text{Cu}$ composite anode for lithium ion batteries", *Journal of Alloys and Compounds*, Vol. 457, pp. 400
81. Ge, H., Li, N., Li, D., Dai, C. and Wang, D., 2008, "Study on the effect of Li doping in spinel $\text{Li}_{4+x}\text{Ti}_{5-x}\text{O}_{12}$ ($0 \leq x \leq 0.2$) materials for lithium-ion batteries", *Electrochemistry Communication*, Vol. 10, pp. 1031-1034
82. Ji, S., Zhang, J., Wang, W., Huang, Y., Feng, Z., Zhang, Z. and Tang, Z., 2010, "Preparation and effects of Mg-doping on the electrochemical properties of spinel $\text{Li}_4\text{Ti}_5\text{O}_{12}$ as anode material for lithium ion battery", *Material Chemical Physics*, Vol. 123, pp. 510-515
83. Zhao, H., Li, Y., Zhu, Z., Lin, J., Tian, Z. and Wang, R., 2008, "Structural and electrochemical characteristics of $\text{Li}_{4-x}\text{Al}_x\text{Ti}_5\text{O}_{12}$ as anode material for lithium-ion batteries", *Electrochemical Acta*, Vol. 53, pp. 7079-7083
84. Huang, S., Wen, Z., Zhu, X. and Z. Lin, 2007, "Effects of dopant on the electrochemical performance of $\text{Li}_4\text{Ti}_5\text{O}_{12}$ as electrode material for lithium ion batteries", *Journal of Power Sources*, Vol. 165, pp. 408-412
85. Lin, Z., Hu, X., Huai, Y., Liu, L., Deng, Z. and Suo, J., 2010, "One-step synthesis of $\text{Li}_4\text{Ti}_5\text{O}_{12}/\text{C}$ anode material with high performance for lithium-ion batteries", *Solid State Ionics*, Vol. 181, pp. 412-415
86. Liu, H., Feng, Y., Wang, K., and Xie, J., 2008, "Synthesis and electrochemical properties of $\text{Li}_4\text{Ti}_5\text{O}_{12}/\text{C}$ composite by the PVB rheological phase method", *Journal of Physics and Chemistry of Solids*, Vol. 69, pp. 2037-2040
87. Huang, J. and Jiang, Z., 2008, "The preparation and characterization of $\text{Li}_4\text{Ti}_5\text{O}_{12}/\text{carbon nano-tubes}$ for lithium ion battery", *Electrochemical Acta*, Vol. 53, pp. 7756-7759
88. Li, X., Qu, M., Huai, Y. and Yu, Z., 2010, "Preparation and electrochemical performance of $\text{Li}_4\text{Ti}_5\text{O}_{12}/\text{carbon}/\text{carbon nano-tubes}$ for lithium ion battery", *Electrochemical Acta*, Vol. 55, pp. 2978-2982

89. Cai, R., Yu, X., Liu, X. and Shao, Z., 2010, "XPS and ToF-SIMS study of Sn-Co alloy thin films as anode for lithium ion battery", *Journal of Power Sources*, Vol. 195 pp. 8251-8257
90. Hsiao, K. C., Liao, S. C. and Chen, J. M., 2008, *Electrochemical Acta*, Vol. 53, p. 7242
91. Vasconcelos, D. C. L., Costa, V. C., Nunes, E. H. M., Sabioni, A. C. S., Gasparon, M. and Vasconcelos, W. L., 2011, "Infrared spectroscopy of titania sol-gel coatings on 316L stainless steel", *Materials Sciences and Applications*, Vol. 02(10), pp. 1375-1382
92. Priyono, B., Syahrial, A. Z., Yuwono, A. H., Kartini, E., Marfelly, M. and Rahmatulloh, W. M. F., 2015, "Synthesis of lithium titanate ($\text{Li}_4\text{Ti}_5\text{O}_{12}$) through hydrothermal process by using lithium hydroxide (LiOH) and titanium dioxide (TiO_2) Xerogel", *International Journal of Technology*, Vol. 4 pp. 555-564
93. Nithya, V. D., Selvan, R. K., VEDIAPPAN, K., Sharmila, S. and Lee, C. W., 2012, "Molten salt synthesis and characterization of $\text{Li}_4\text{Ti}_{5-x}\text{Mn}_x\text{O}_{12}$ ($x=0.0, 0.05$ and 0.1) as anodes for Li-ion batteries", *Applied Surface Science*, Vol. 261, pp. 515-519
94. Borghols, W. J. H., Wagemaker, M., Lafont, U., Kelder, E. M. and Mulder, F. M., 2009, "Size Effects in the $\text{Li}_{4+x}\text{Ti}_5\text{O}_{12}$ Spinel", *Journal of the American Chemical Society*, Vol. 131, p.17786
95. Kubiak, P., Garcia, A., Womes, M., Aldon, L., Fourcade, J. O., Lippens, P. E. and Jumas, J. C., 2003, *Journal of Power Sources*, Vol. 119, p. 626
96. Makimura, Y. and Ohzuku, T., 2009, In *Encyclopedia of Electrochemical Power Sources*, (Eds: x00Fc, G.rgen), Elsevier, Amsterdam, p. 249
97. Liu, D., Ouyang, C., Shu, J., Jiang, J., Wang, Z. and Chen, L., 2006, *Physical Status Solidi (b)*, Vol. 243, p. 1835
98. Ge, H., Li, N., Li, D., Dai, C. and Wang, D., 2009, "Study on the Theoretical Capacity of Spinel Lithium Titanate Induced by Low-Potential Intercalation", *The Journal of Physical Chemistry C*, Vol. 113, pp. 6324
99. Shu, J., 2009, "Electrochemical behavior and stability of $\text{Li}_4\text{Ti}_5\text{O}_{12}$ in a broad voltage window", *Journal of Solid State Electrochemistry*, Vol.13, p.1535

100. Jovic, N., Antic, B., Kremenovic, A., Spasojevic-de Bire, A. and Spasojevic, V., 2003, *Physical Status Solidi (a)*, Vol. 198, p. 18
101. Zhong, Z., Ouyang, C., Shi, S. and Lei, M., 2008, *Chemical Physical Chemistry*, Vol. 9, p. 2104
102. Kosova, N. V., Devyatkina, E. T., Anufrienko, V. F., Vasenin, N. T., Vosel and Khim, S. V. T. V. L., 2002, *Interesakh Ustoich. Razvit.*, Vol 10, p. 127
103. Sorensen, E. M., Barry, S. J., Jung, H. K., Rondinelli, J. R., Vaughey, J. T. and Poeppelmeier, K. R., 2006, *Chemistry of Materials*, Vol. 18, p. 482
104. Wagemaker, M., Eck, E. R. H. V., Kentgens, A. P. M. and Mulder, F. M., 2009, *Journal of Physical Chemistry B*, Vol. 113, p. 224
105. Wilkening, M., Amade, R., Iwaniak, W. and Heitjans, P., 2007, *Physical Chemistry Chemical Physics*, Vol. 9, p. 1239
106. Leonidov, I., Leonidova, O., Perelyaeva, L., Samigullina, R., Kovyazina, S. and Patrakeev, M., 2003, *Physics of the Solid State*, Vol. 45, p. 2183
107. Scharner, S., Weppner, W. and Beurmann, S., 1999, *Journal of Electrochemical Society*, Vol. 146, pp. 258-262